------- Iraqi National Journal of Earth Sciences, Vol. 13, No. 1, pp. 75 – 102, 2013-------

# Fault-slip Analysis and Paleostress Reconstruction at Sara Anticline-Dokan Dam Site Northeastern Iraq

**Ibrahim S. Al-jumaily**
*Department of Geology*
*College of Science*
*University of Mosul*

**Saddam I. Al-khatoni**
*Department of Geology*
*College of Science*
*University of Mosul*

(Received 30/8/2012 , Accepted 26/2/2013)

## ABSTRACT

Stress inversion of fault-slip data has been worked by application of improved Right- Dihedral technique, succeeded by rotational optimization (Win-Tensor Software of Delvaux, 2010, version 2.2.3). Attitudes of fault planes, striations and their movement sense, were gathered from quarries and road cut exposures of carbonate rocks at Sara anticline situated in the high fold belt of northeastern Iraq. The obtained paleostress tensors of the current fault-slip analysis are (according to the general trends of $\delta_1$ (**δHmax**.) for strike slip and compressive tensors and $\delta_3$ **(δHmin.)** for extensional tensors): NNE-SSW, NE-SW primary strike slip and compressive tensors; WNW-ESE, NW-SE, NNW-SSE strike slip and compressive subordinate (relaxed) tensors; NW-SE extensional tensor byproduct from the primary tensor sets; and NNE-SSW, NE-SW extensional tensors associated with releasing phase accompanying the final uplift of the main fold. The multitrends of the computed paleostress tensors might be attributed to the oblique convergence and collision of Arabian and Iranian plates along their zigzaged margins.

**Keywords**: Fault-slip, Paleostress, Reconstruction, Sara, Dokan Dam,Iraq.

---

# تحليل انزلاق الفوالق وبناء الاجهاد القديم في طية سارة المحدبة - موقع سد دوكان - شمال شرق العراق

**ابراهيم سعد ابراهيم الجميلي**
*قسم علوم الأرض*
*كلية العلوم*
*جامعة الموصل*

**صدام عيسى الخاتوني**
*قسم علوم الأرض*
*كلية العلوم*
*جامعة الموصل*

**الملخص**

أجري تحليل الاجتهاد القديم من بيانات الفوالق الموسمة أسطحها بحزوز الصفاح بتطبيق تقنية الأوجه المتعامدة المحسنة ومن ثم الأمثلية الدورانية (برنامج Win-Tensor للباحث Delvaux, 2010, الإصدارية 2.2.3 )، وذلك في طية سارة المحدبة الواقعة في نطاق الطيات العالية شمال شرقي العراق. جمعت قياسات الوضعية لأعداد كبيرة من مستويات الفوالق ولحزوز الصفاح فيها وبيانات اتجاه وطبيعة الحركة عليها من بعض المقالع ومكاشف قطع الطريق للصخور الكاربوناتية. تنسرات الاجهاد القديم المستنبطة من التحليل الحالي (طبقا للاتجاهات العامة لمحور الاجهاد الأفقي الأعظم لتنسرات الازاحة المضربية والانضغاطية (**δHmax.**) **$\delta_1$** والأدنى **(δHmin.)** **$\delta_3$** للتنسرات التمددية) هي: تنسرات إزاحة مضربية وإنضغاطية رئيسية، محور الاجهاد الاعظم فيها يتخذ اتجاهي NNE-SSW, NE-SW وتنسرات إزاحة مضربية وإنضغاطية ثانوية (طور الارتخاء الذي يعقب طور الانضغاط للنبضة التكتونية)، محور الاجهاد الاعظم فيها يتخذ اتجاهات WNW-ESE, NW-SE, NNW-SSE وتنسر تمددي كناتج عرضي لتنسرات الإزاحة المضربية والانضغاطية الرئيسية وبمحور إجهاد أدنى باتجاه NW-SE وتنسران تمددیان يعودان لطور الارتخاء المصاحب للرفع النهائي للطية الرئيسة وبمحور إجهاد أدنى باتجاهي NNE-SSW, NE-SW. إن تعدد إتجاهات تنسرات الاجهاد القديم المستنتجة في هذه الدراسة قد يعزى إلى التصادم المائل وبحافات متعرجة بين الطبقين العربي والايراني.

**الكلمات الدالة:** انزلاق الفوالق، الإجهاد القديم، سارة، سد دوكان، العراق.

---

## INTRODUTION

The aim of present investigation is to detect the paleostress states responsible for structural configuration and hence to unravel the stress state evolution of Sara anticline about 30km. northwest Sulaimaniya Governorate/Kurdistan Region, northeastern Iraq. The study area is located within high fold zone of Zagros Fold-Thrust Belt of Iraq (Fig. 1). Structurally it is a NW-SE extension of the major Surdash anticline, foreland (SW) verging, WNW-ESE trending asymmetrical anticline (Fig. 2 and 3). Stratigraphically it comprises exposures of rocks units extending from middle Cretaceous to end Pliocene (Fig. 2).

Many paleostress inversion procedures were developed using graphical and analytical means (Angelier *et al.,* 1982; Angelier, 1984; 1990; 1994). During the last three decades, paleostress inversion techniques have been applied to various tectonic settings and have proved its empirical validity and successful, although the presence

of certain limitations (Pollard *et al.,* 1993; Nemcok and Lisle, 1997; Twiss and Unruh, 1998). Most of the analytical techniques apply the assumption of (Wallace 1951, and Bott, 1959), that is the slip occurs parallel to the maximum resolved shear stress on a pre-existing and/or newly formed fault plane.

In the present investigation, three techniques of fault slip analysis were used:

1- Compression (P) and tension (T) axes method (Turner, 1953 in Angellier, 1994), traditionally known as PBT technique, where P: is maximum principal stress axis $\boldsymbol{\delta_1}$, B: intermediate principal stress axis $\boldsymbol{\delta_2}$, and T: minimum principal stress axis $\boldsymbol{\delta_3}$. The $\boldsymbol{\delta_1}$ (P axis) and $\boldsymbol{\delta_3}$ (T axis) are at 45° on either side of slip lineation contained in a plane normal to fault plane, whereas $\boldsymbol{\delta_2}$ lies within fault plane and normal to the plane containing $\boldsymbol{\delta_1}$ and $\boldsymbol{\delta_3}$ axes.

2- The right dihedral technique (Angelier and Mecheler, 1977): two pairs of opposite facets formed via stereographic projection of the fault plane and its orthogonal auxiliary plane. The maximum principal stress axis $\boldsymbol{\delta_1}$ lies within two opposite facets named pressure dihedral, whereas the minimum principal stress axis $\boldsymbol{\delta_3}$ lies within the other pair of facets named tension dihedral. The specification of such dihedral is dependent upon the sense of slip on the fault surface. The pressure and tension fields are reduced by progressive superimposing of facets through plotting excessive numbers of faults and their auxiliary planes, and eliminating uncommon portions. The geometric centers of the final pressure and tension areas are taken as $\boldsymbol{\delta_1}$ and $\boldsymbol{\delta_3}$ locations respectively. The $\boldsymbol{\delta_2}$ attitude is then determined as normal to the plane containing $\boldsymbol{\delta_1}$ and $\boldsymbol{\delta_3}$ axes.

3- The Rotational Optimization technique (Delvaux and Sperner, 2003): the solutions obtained by either of the previous techniques are processed in iterative way. At each run, one of the principal stress axes of the input tensor is fixed and either of the other two axes is rotated successively around the fixed one with a number of angles until a most stable tensor is gained. Further, the stress ratio of such a tensor is also optimized through a range of values until a most stable ratio is reached. The remained incompatible data is removed from the characteristic data set of this final optimized tensor.

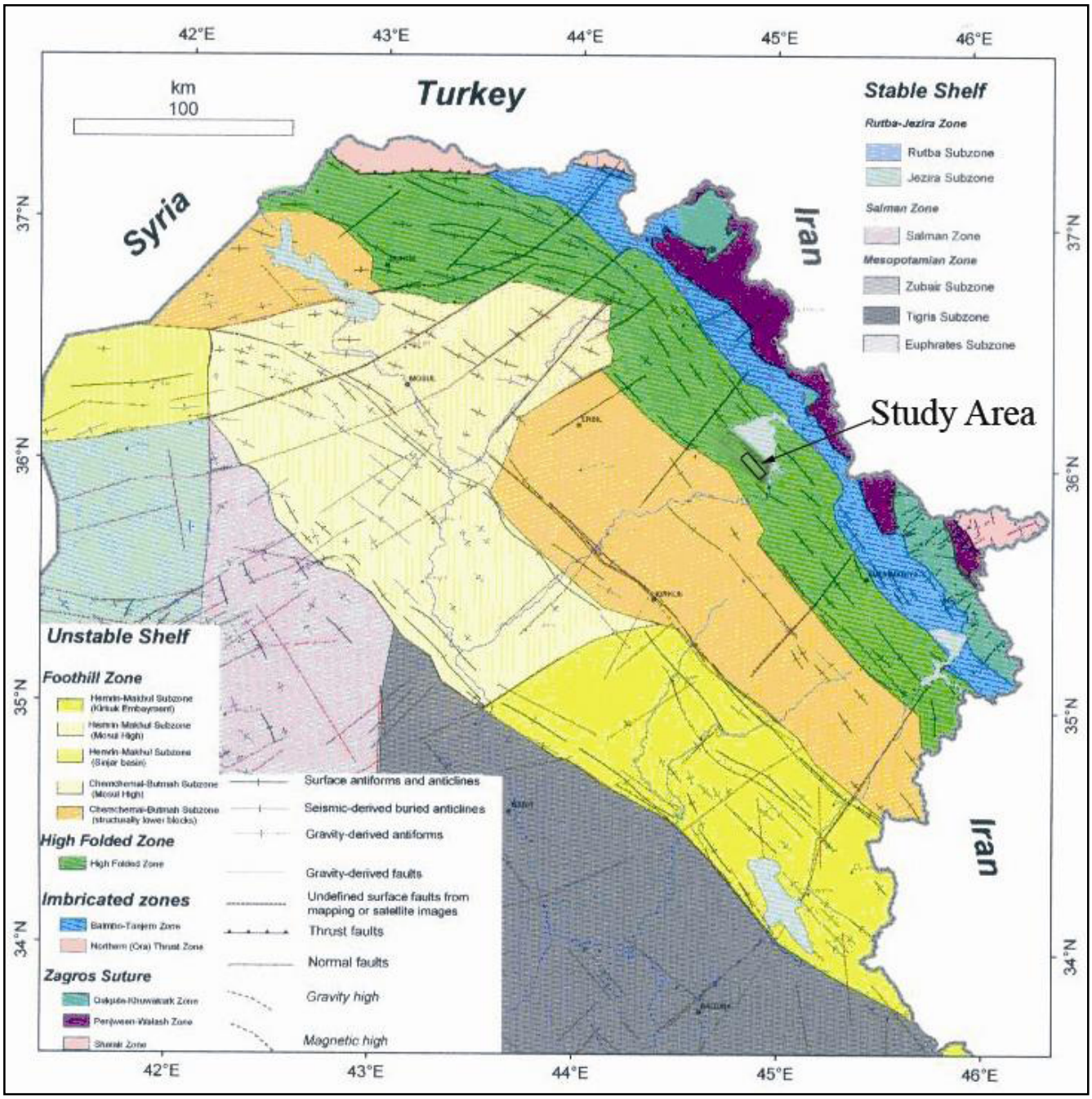


Fig. 1: Tectonic Map of Northern Iraq Showing Location of Study Area (Jassim and Goff, 2006).

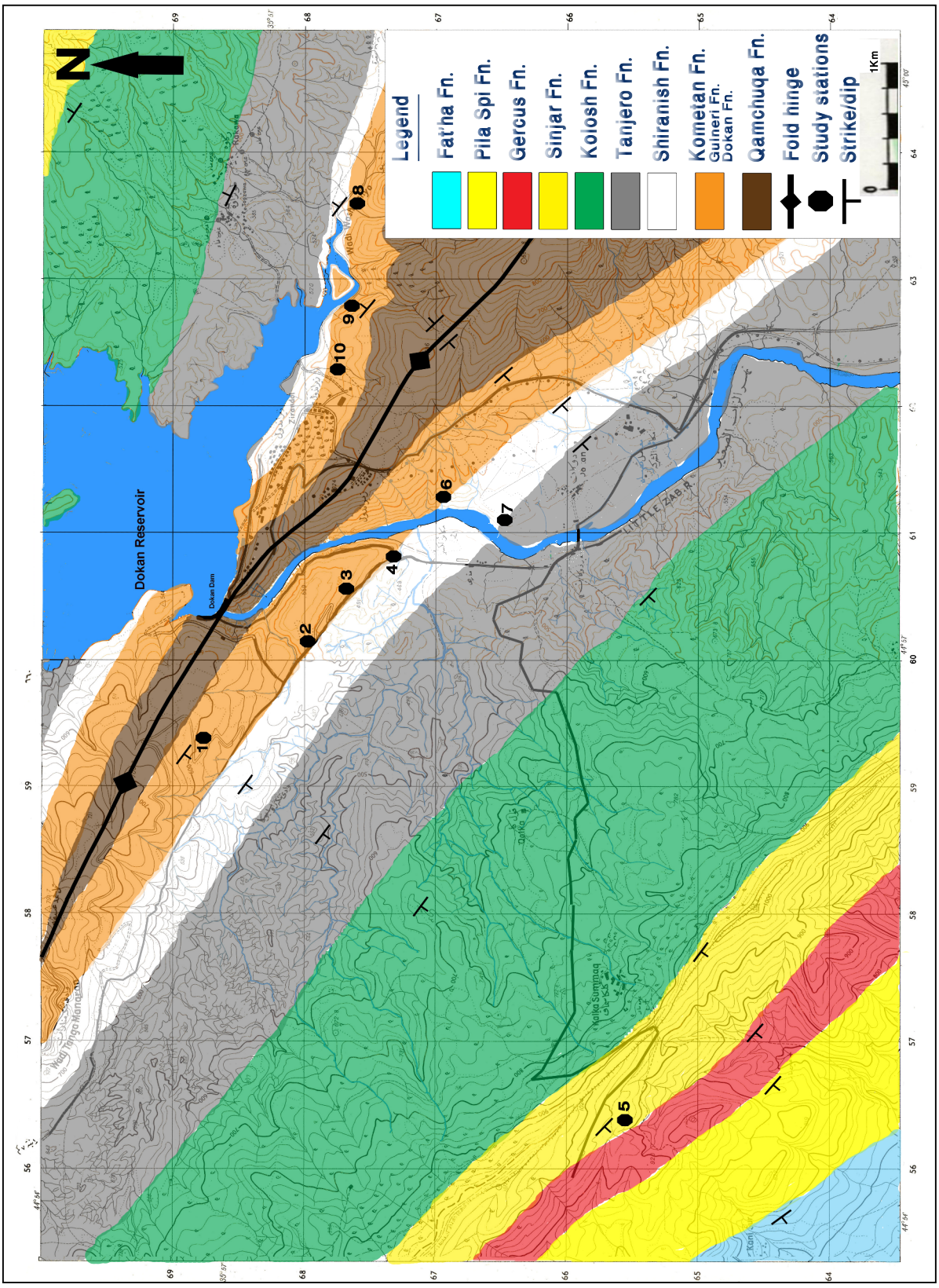


Fig. 2: Geological Map of Study Area.

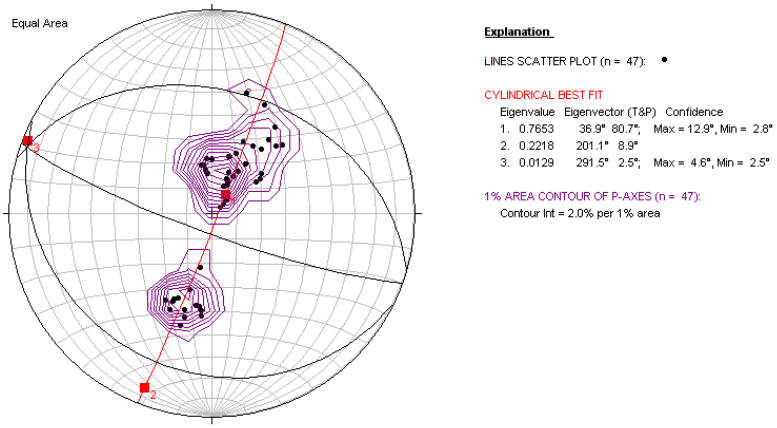


Fig. 3: Contoured PI-Diagram of Sara Anticline.

## INVESTIGATION PROCEDURE AND ANALYSIS TECHNIQUE

Field data and measurements of mesoscopic faults were collected from 10 field stations distributed mainly within Late Cretaceous Kometan formation (8 stations), and only (2) stations in Tanjero (Late Cretaceous) and Sinjar (Paleocene) formations (Fig. 2). The global positions of investigated sites were fixed using portable GPS apparatuse. In each site, attitudes of bedding and fault planes were taken using Silva compass with strike azimuth clockwise from dip direction. The acute, Pitch (rake) angle of slip lines on striated planes measured with notation to the strike end orientation of the fault plane. Beside that, the sense of slip on each surface was estimated with the aid of available kinematic indicaters. Furthermore, field photographes and sketches were done for interesting features, as well as necessary field notes and interpretations were registered for them.

The gathered data were processed using PBT, Right Dihedra and Rotational Optimization techniques successively. These techniques are involved in Win_Tensor software of Delvaux version 2.2.3. At first the data of each station were treated separately just by applying PBT technique. This step of analysis had provided a preliminary assesment of the number and types of both prevailing and subordinate paleostress tensors in study area. The parameters of each tensor consist of attitudes of the three principal stress axes : maximum δ1, intermediate δ2 and minimum δ3, and a stress ratio R according to (Angelier, 1984; 1990; 1994; Angelier *et al.,* 1982; ). In the second step, data groups of the same or closer tensors from whole stations were processed simultaneously using PBT technique again. The step was repeated using Right Dihedra technique. In the third step, the tensors obtained from previous step were optimized through dynamic rotation of two of tensor axes around the third one

for a number of degrees each time. The process involves a likelyhood optimization for stress ratio also.The procedure is performed by chossing aspecific algorithim (Delvaux and Sperner, 2003).The most stable tensor then specified for each group of data.

## GEOMETRIC CONFIGURATION OF MESOSCOPIC FAULTS IN STUDY AREA

A total number of 180 striated mesoscopic fault planes were measured throughout the 10 field stations. Their trends vary through 360º, likewise their dips range from low to high angles (Fig. 4 and 5). Thus their planes take all geometrical configurations with respect to bedding attitudes in the area (i.e strike, dip and oblique). However, according to their slip sense, they are categorized into more preavalent strike slip (Photo 1) and substantial normal (Photo 2) and reverse slip (Photo 3) mesoscopic faults. Their areal and vertical extensions range from a few square centimeters to several tens of meters. They are mostly planar but some show curved surfaces. Most of them have even polished surfaces but others are uneven, and some shows pitted sectors indicating transpression (Phot 4), whereas others express extension sectors (calcite growth) which indicate transtension (Photo 5). Most of striated surfaces show step facets which aid in considering their sense of slip (photo 1). The clearnes of slickensides on striated surfaces range from very slight to very prominent. Some planes show two cross cutting striation sets (photo 6) which might refer to temporal succession of their causative stress tensors.

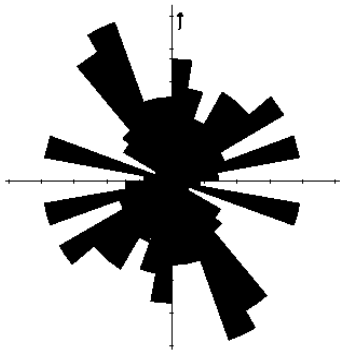

Fig. 4: Rose-Diagram of Mesofaults Ttrends in Sara Anticline.

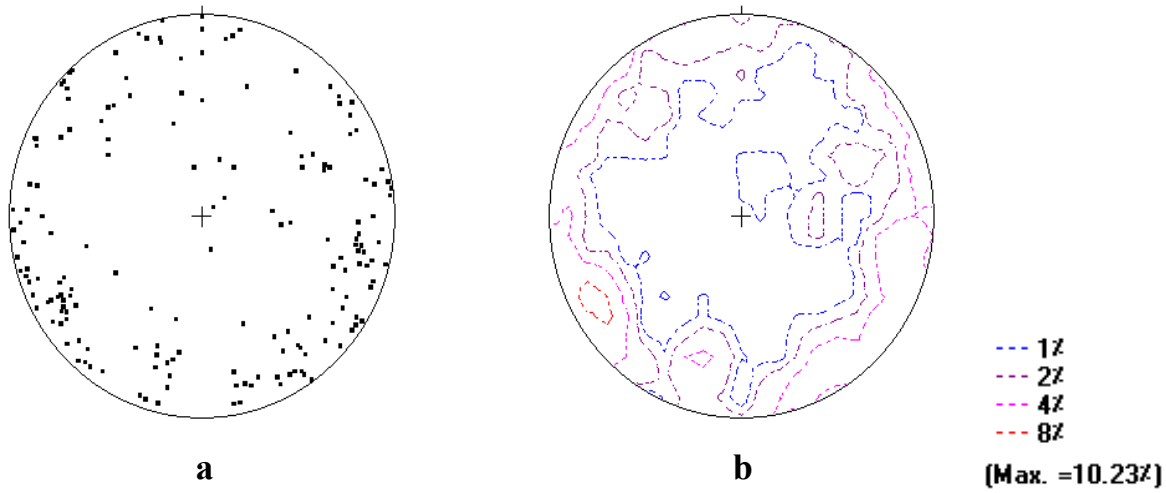


Fig. 5: **a:** Scattered and **b:** Contoured Poles of Mesofaults in Sara Anticline

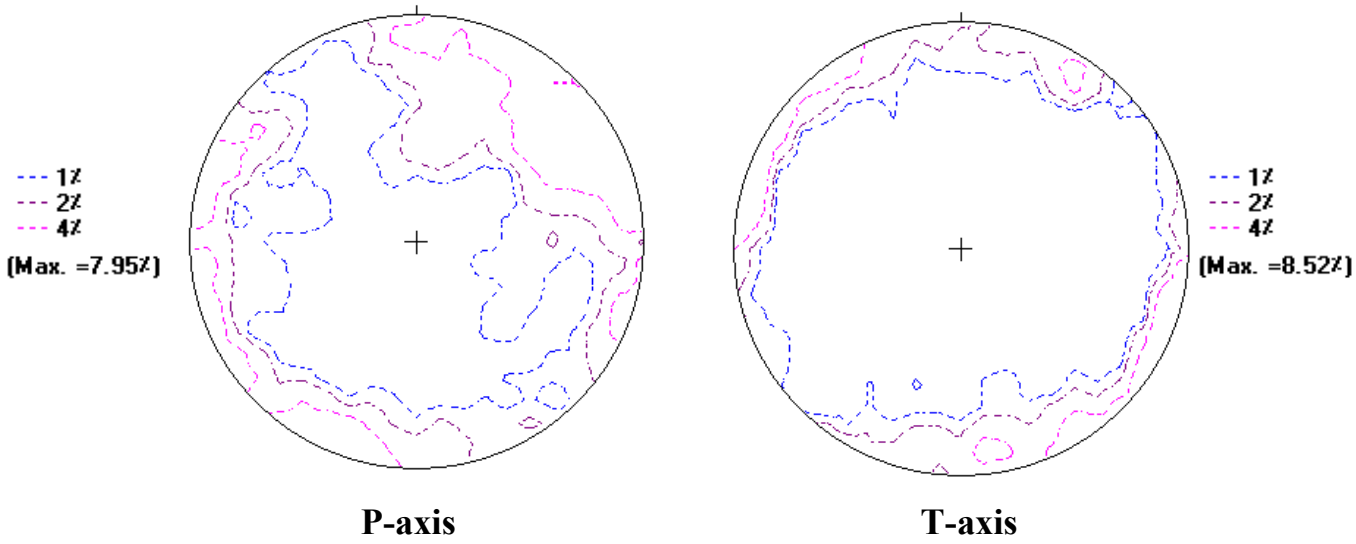


Fig. 6: Contoured **P** and **T** Axes Deduced from Mesofaults in Sara Anticline

## KINEMATIC ANALYSIS OF FAULT SLIP DATA

A preliminary assesment of maximum and minimum kinematic axes (P and T axes) attitudes for whole fault slip data was performed collectively using GEORIENT software. The contoured outputs of this analysis show a wide range orientations of the both axes (Fig. 6). This indicates that the study area had been subjected to several stress tensors throughout the tectonic development. Therefore the kinematic analysis of the fault slip data was progressed in the following steps to elucidate such those stress tensors.

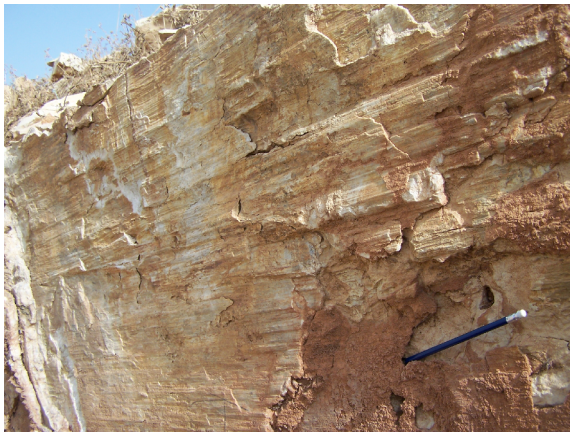

Photo 1: Prominent striated surface of a sinistral strike slip fault in Kometan Fm. at station 1.

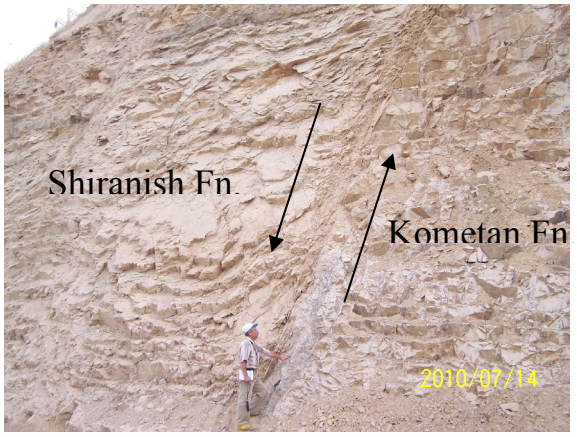


Photo 2- A transverse normal slip fault juxtaposing Kometan and Shiranish Fms. at station 4.


Photo 3-Antithetic reverse slip fault disrupting beds of Kometan Fm. at station 7.

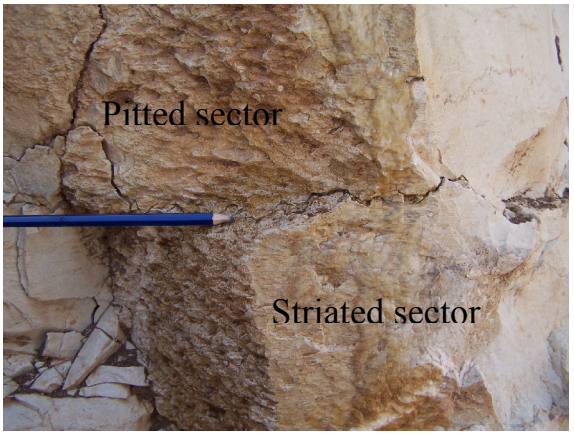


Photo 4-A transpressive fault showing both shear (striations) and compression (pitted) facets in Kometan Fm. at station 1.

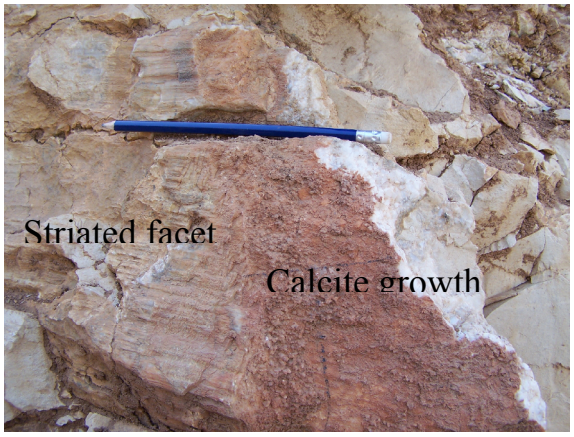


Photo 5- A transtensive fault showing both shear (striations) and extension (calcite growth) facets in Kometan Fm. at station 1.

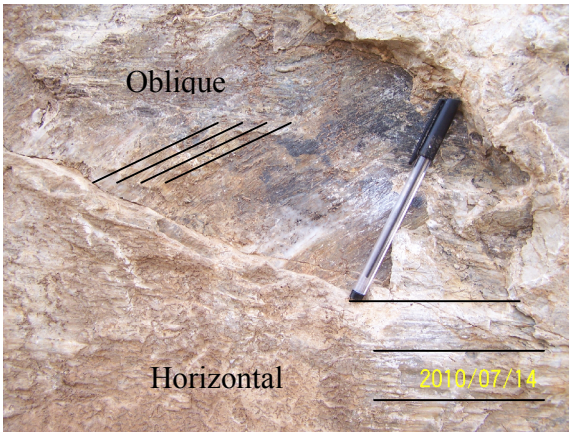


Photo 6- Superimposed slickenside sets on a sinistral fault surface in Kometan Fm. at station 4. The younger with almost horizontal striations, whereas the older pitching 31° with fault strike.

**Step I**

In this step, fault slip data of each field station were analysed separately by applying PBT fault slip analysis technique which is built in Win -Tensor software of Delvaux (version 2.2.3) as stated before. The parametars of the computed paleostress tensors are shown in tables (1,2 and 3). They are listed according to the general azimuth of their greatest (strike slip and compressive tensors) or least principal stress axes (extension tensors):

**A-** Strike slip tensors:

Table 1: Parameters of Strike Slip Paleostress Tensors as Deduced by PBT Analysis of Strike Slip Mesofaults in Study Stations.

| Station No. | Faults no. | Principal stresses attitudes | | | R | R` | α | δH max. | δH min. |
|---|---|---|---|---|---|---|---|---|---|
| | | $\delta_1$ | $\delta_2$ | $\delta_3$ | | | | | |
| 2 | 2 | 186/14 | 350/75 | 095/04 | 0.5 | 1.5 | 4.4 | 006 | 096 |
| 3 | 4 | 356/02 | 102/82 | 266/07 | 0.5 | 1.5 | 11.1 | 177 | 087 |
| 4 | 4 | 005/16 | 124/59 | 267/26 | 0.57 | 1.43 | 15.4 | 001 | 091 |
| 1 | 17 | 213/05 | 005/85 | 123/03 | 0.5 | 1.5 | 18.5 | 033 | 123 |
| 6 | 5 | 015/25 | 141/50 | 271/28 | 0.57 | 1.43 | 17.3 | 008 | 098 |
| 6 | 5 | 031/21 | 270/54 | 134/28 | 0.5 | 1.5 | 21.8 | 038 | 128 |
| 7 | 6 | 018/26 | 211/63 | 111/05 | 0.56 | 1.44 | 20.1 | 020 | 110 |
| 10 | 13 | 011/04 | 172/85 | 281/02 | 0.52 | 1.48 | 12 | 011 | 101 |
| 3 | 8 | 234/01 | 327/65 | 144/25 | 0.5 | 1.5 | 16.2 | 055 | 145 |
| 3 | 1 | 047/19 | 173/59 | 308/23 | 0.5 | 1.5 | | 043 | 133 |
| 9 | 13 | 042/38 | 203/50 | 305/10 | 0.48 | 1.52 | 15.5 | 038 | 128 |
| 9 | 2 | 220/26 | 012/61 | 124/12 | 0.56 | 1.44 | 16.7 | 036 | 126 |
| 2 | 12 | 068/05 | 293/83 | 159/05 | 0.5 | 1.5 | 19.8 | 068 | 158 |
| 4 | 2 | 245/14 | 067/76 | 335/00 | 0.48 | 1.52 | 13 | 065 | 155 |
| 8 | 1 | 073/22 | 188/46 | 326/35 | 0.5 | 1.5 | | 066 | 156 |
| 10 | 1 | 062/33 | 265/55 | 159/11 | 0.5 | 1.5 | | 066 | 156 |
| 1 | 8 | 092/01 | 357/84 | 182/06 | 0.47 | 1.53 | 18 | 092 | 002 |
| 5 | 2 | 262/26 | 046/58 | 164/16 | 0.39 | 1.61 | 29.5 | 080 | 170 |
| 6 | 2 | 276/31 | 156/41 | 030/34 | 0.52 | 1.48 | 7 | 109 | 019 |
| 7 | 1 | 274/11 | 016/48 | 175/40 | 0.5 | 1.5 | | 090 | 000 |
| 2 | 3 | 299/07 | 106/83 | 209/02 | 0.47 | 1.53 | 15.1 | 119 | 029 |
| 4 | 4 | 300/17 | 103/72 | 210/05 | 0.53 | 1.47 | 9.2 | 120 | 030 |
| 10 | 7 | 110/09 | 327/79 | 201/07 | 0.47 | 1.53 | 16.2 | 110 | 020 |
| 7 | 2 | 131/18 | 267/66 | 036/16 | 0.61 | 1.39 | 16 | 128 | 038 |
| 6 | 4 | 153/08 | 260/63 | 060/26 | 0.37 | 1.63 | 28 | 153 | 063 |
| 8 | 1 | 334/04 | 236/64 | 066/26 | 0.5 | 1.5 | | 155 | 065 |
| 10 | 1 | 327/29 | 168/59 | 062/09 | 0.5 | 1.5 | | 150 | 060 |

**B-** Compressive tensors

Table 2: Parameters of Compression Paleostress Tensors as Deduced by PBT Analysis of Reverse Slip Mesofaults in Study Stations.

| Station No. | Faults no. | Principal stresses attitudes | | | R | R` | α | δH max. | δH min. |
|---|---|---|---|---|---|---|---|---|---|
| | | $\delta_1$ | $\delta_2$ | $\delta_3$ | | | | | |
| 3 | 1 | 022/13 | 115/12 | 244/72 | 0.5 | 2.5 | | 019 | 109 |
| 5 | 1 | 194/18 | 286/07 | 038/71 | 0.5 | 2.5 | | 011 | 101 |
| 1 | 1 | 040/18 | 310/03 | 212/72 | 0.5 | 2.5 | | 041 | 131 |
| 2 | 3 | 054/09 | 324/05 | 204/79 | 0.57 | 2.57 | 19.2 | 056 | 146 |
| 6 | 5 | 055/32 | 160/21 | 277/50 | 0.48 | 2.48 | 14 | 041 | 131 |
| 8 | 4 | 039/34 | 296/19 | 182/50 | 0.47 | 2.47 | 16.6 | 055 | 145 |
| 9 | 4 | 041/09 | 309/19 | 157/68 | 0.55 | 2.55 | 13.5 | 045 | 135 |
| 10 | 2 | 081/21 | 343/23 | 210/58 | 0.5 | 2.5 | 9.6 | 090 | 000 |
| 4 | 1 | 289/09 | 192/36 | 031/53 | 0.5 | 2.5 | | 112 | 022 |
| 9 | 1 | 114/10 | 017/34 | 219/54 | 0.5 | 2.5 | | 118 | 028 |
| 9 | 5 | 301/18 | 197/41 | 049/44 | 0.5 | 2.5 | 10.2 | 128 | 038 |
| 4 | 2 | 161/28 | 265/25 | 032/51 | 0.5 | 2.5 | 9 | 149 | 059 |

**C-** Extension tensors

Table 3: Parameters of Extension Paleostress Tensors as Deduced by PBT Analysis of Normal Slip Mesofaults in Study Stations.

| Station No. | Faults no. | Principal stresses attitudes | | | R | R` | α | δH max. | δH min. |
|---|---|---|---|---|---|---|---|---|---|
| | | $\delta_1$ | $\delta_2$ | $\delta_3$ | | | | | |
| 2 | 3 | 025/75 | 278/04 | 187/14 | 0.66 | 0.66 | 22.2 | 096 | 006 |
| 3 | 1 | 117/47 | 311/42 | 214/07 | 0.5 | 0.5 | | 122 | 032 |
| 6 | 5 | 324/52 | 144/38 | 234/00 | 0.5 | 0.5 | 14 | 144 | 054 |
| 4 | 1 | 012/72 | 169/16 | 260/06 | 0.5 | 0.5 | | 172 | 082 |
| 7 | 1 | 188/40 | 357/49 | 093/05 | 0.5 | 0.5 | | 005 | 095 |
| 8 | 1 | 028/44 | 188/44 | 288/10 | 0.5 | 0.5 | | 022 | 112 |
| 1 | 2 | 049/54 | 233/36 | 142/02 | 0.5 | 0.5 | 12 | 051 | 141 |
| 3 | 5 | 061/78 | 233/12 | 324/02 | 0.43 | 0.43 | 16 | 054 | 144 |

**Step 2**

In this step of kinematic analysis, the whole fault slip data from all field stations were tested collectively in twice. This was done using PBT and Right dihedral techniques respectively. In both techniques the whole data are searched successively for a specific tensor, and at each time the incompatible data are tested for another tensor and so on. Eventually the whole data are categorized into sets each of which characterized with a specific stress tensor. The base for separation into sets is somewhat different for the two techniques of analysis. In PBT technique, the basis is the angle **α** between synthetically shear stress vector derived from a specific stress tensor and the slip vector on each striated plane. The threshold value of this angle had been taken **30º.** Whereas in the second iterative technique (Right dihedral), the basis for separation of data into tensor sets is the counting deviation (CD) criterion. This is a statistical parameter which defines the mean variance between principal stress axes corresponding to the actual slip vector on each striated surface and the theoretical ones according to a specified stress tensor. Tables (4 and 5) and figures (7-29) illustrate the paleostress tensors obtained by the two analytical techniques cited above.

**A-** Paleostress tensors according to PBT analysis:

Table 4: Elements of Paleostress Tensors in Study Area as a Whole Using PBT Aanalysis

| No. | Faults no. | Principal stresses attitudes | | | R | R` | Q R W | α | Tensor Type | δH max. | δH min. | Fig. |
|---|---|---|---|---|---|---|---|---|---|---|---|---|
| | | $\delta_1$ | $\delta_2$ | $\delta_3$ | | | | | | | | |
| 1 | 58 | 023/04 | 223/86 | 114/01 | 0.5 | 1.5 | C | 19.8 | P. Str | 024 | 114 | 7 |
| 2 | 10 | 242/03 | 343/73 | 152/16 | 0.56 | 1.44 | E | 23.7 | P. Str | 062 | 152 | 8 |
| 3 | 34 | 278/00 | 004/83 | 188/07 | 0.5 | 1.5 | D | 19.5 | P. Str | 099 | 009 | 9 |
| ٤ | 15 | 304/30 | 172/50 | 049/24 | 0.49 | 1.51 | E | 22.2 | P. Str | 132 | 042 | 10 |
| ٥ | 7 | 349/18 | 159/72 | 259/03 | 0.41 | 1.59 | E | 18.5 | P. Str | 169 | 079 | 11 |
| 6 | 9 | 030/14 | 295/20 | 153/65 | 0.5 | 2.5 | E | 16.6 | P.Com | 034 | 124 | 12 |
| 7 | 15 | 055/25 | 148/07 | 252/64 | 0.49 | 2.49 | E | 22.9 | P.Com | 051 | 141 | 13 |
| 8 | 1 | 114/10 | 017/34 | 219/54 | 0.5 | 2.5 | E | | P.Com | 118 | 028 | 14 |
| 9 | 3 | 155/21 | 257/28 | 034/54 | 0.52 | 2.52 | E | 11.9 | P.Com | 147 | 057 | 15 |
| 10 | 3 | 121/48 | 297/41 | 029/02 | 0.5 | 0.5 | E | 12.6 | Ob.Ext | 120 | 030 | 16 |
| 11 | 2 | 165/41 | 327/48 | 067/09 | 0.44 | 1.56 | E | 21.6 | Ob.Ext | 160 | 070 | 17 |
| 12 | 18 | 041/52 | 201/36 | 299/10 | 0.45 | 0.45 | E | 18.7 | P. Ext | 033 | 123 | 18 |
| 13 | 5 | 005/81 | 257/03 | 166/08 | 0.48 | 0.48 | E | 17.6 | P. Ext | 076 | 166 | 19 |

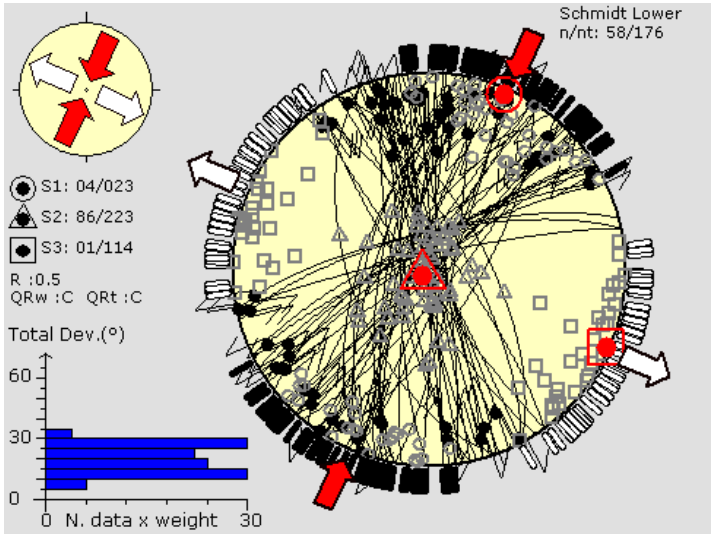


Fig. 7: NNE-SSW strike slip tensor

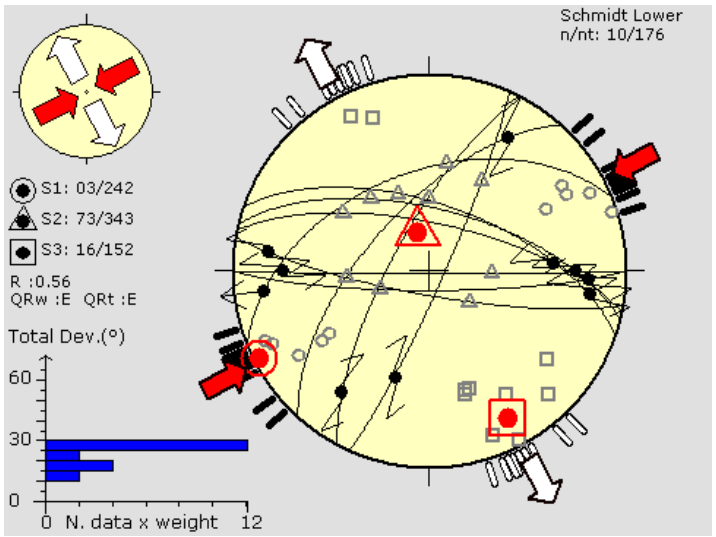


Fig. 8: NE-SW strike slip tensor

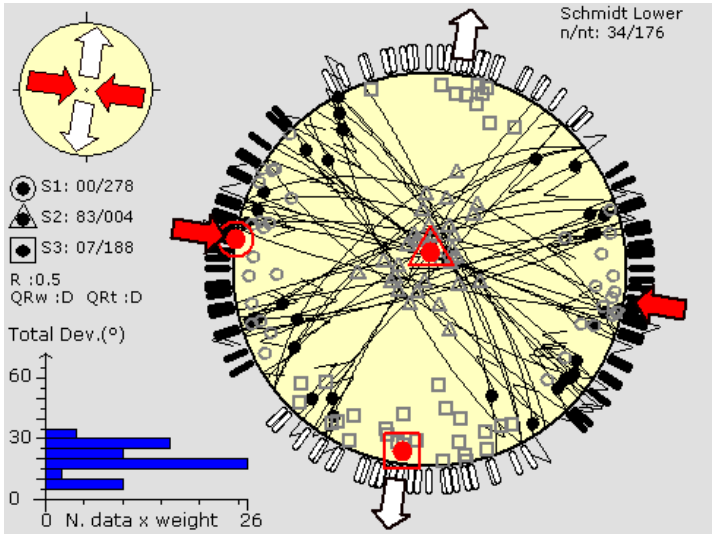


Fig. 9: WNW-ESE strike slip tensor

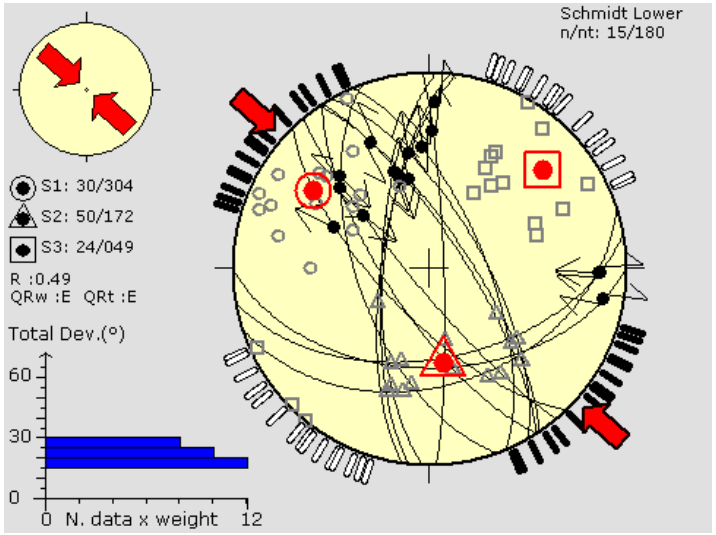


Fig. 10: NW-SE strike slip tensor

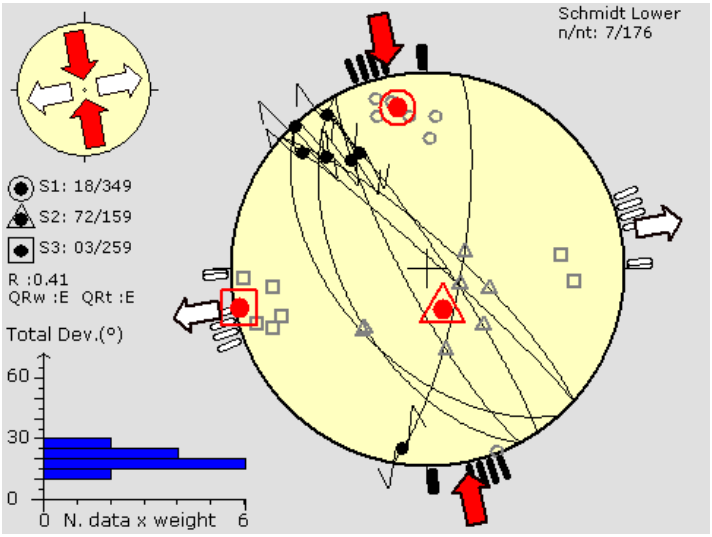


Fig. 11: NNW-SSE strike slip tensor

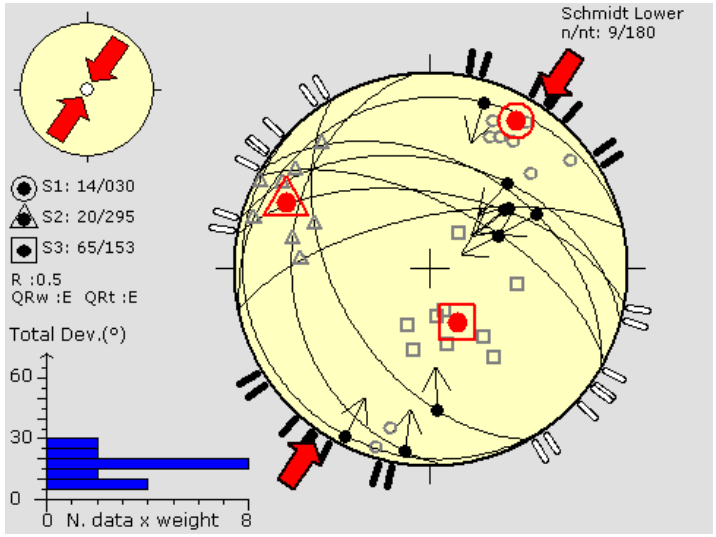


Fig. 12: NNE-SSW compressive tensor

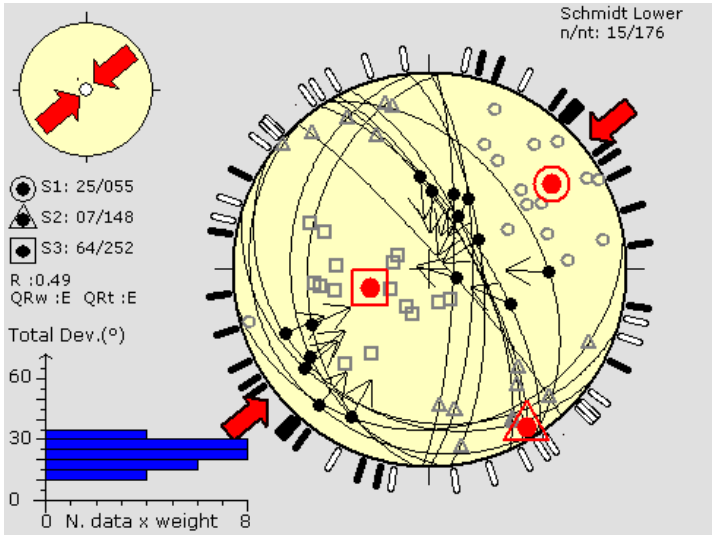


Fig. 13: NE-SW compressive tensor

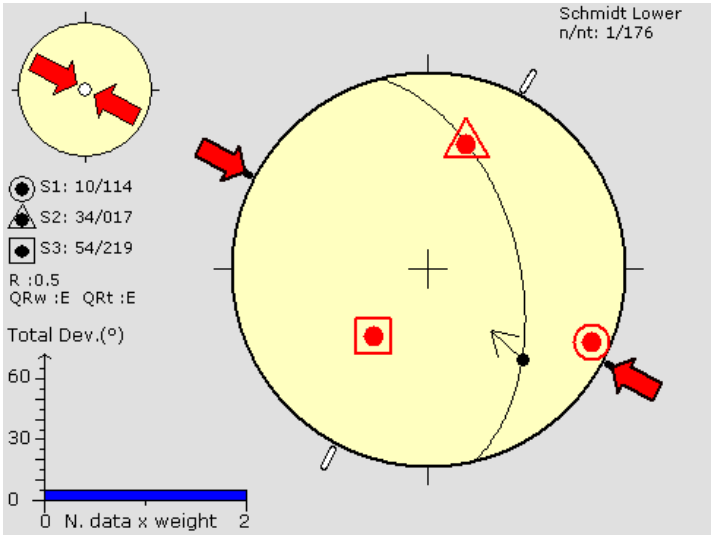


Fig. 14: WNW-ESE compressive tensor

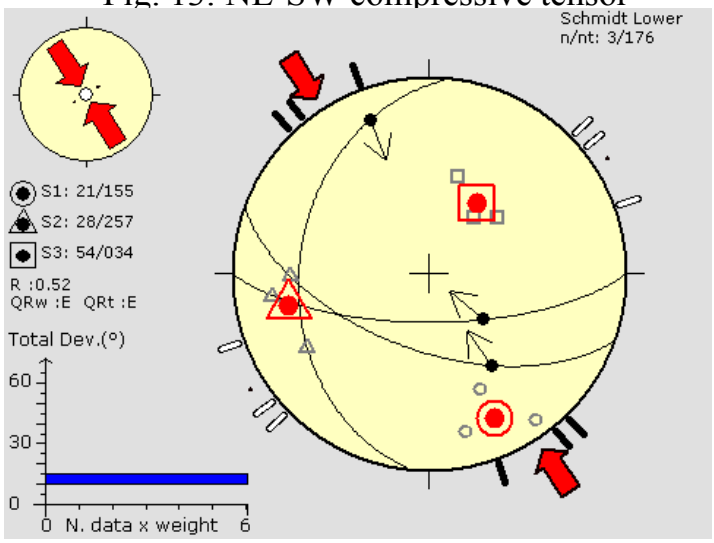


Fig. 15: NW-SE compressive tensor

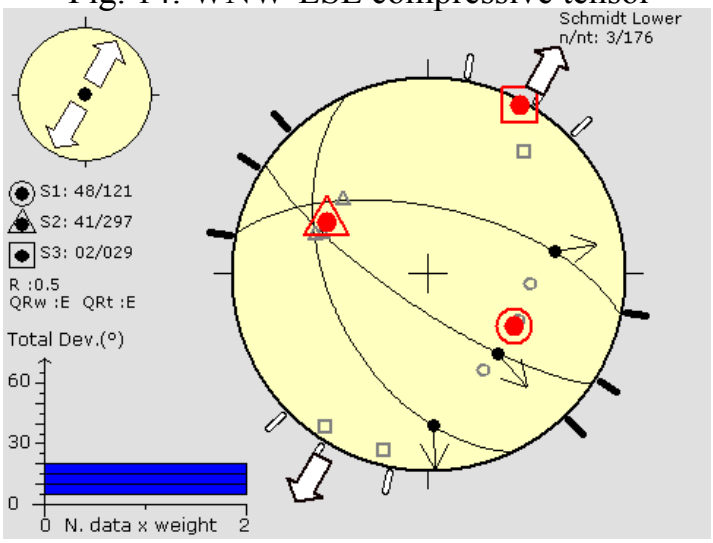


Fig. 16: NNE-SSW extension tensor

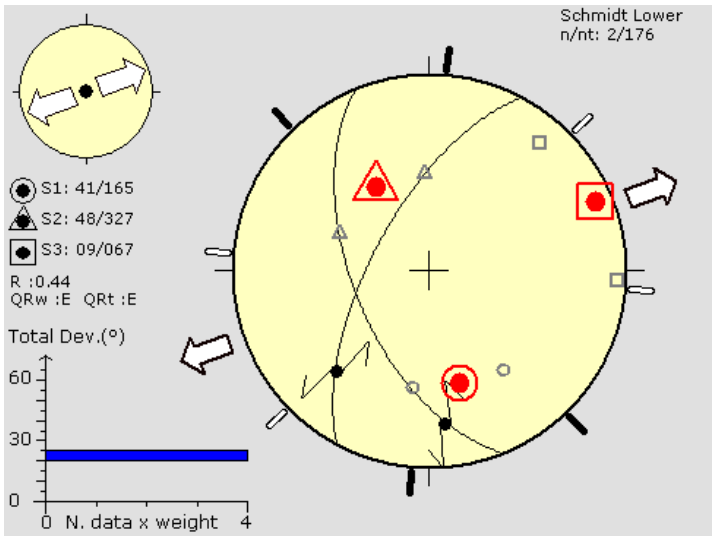


Fig. 17: ENE-WSW extension tensor

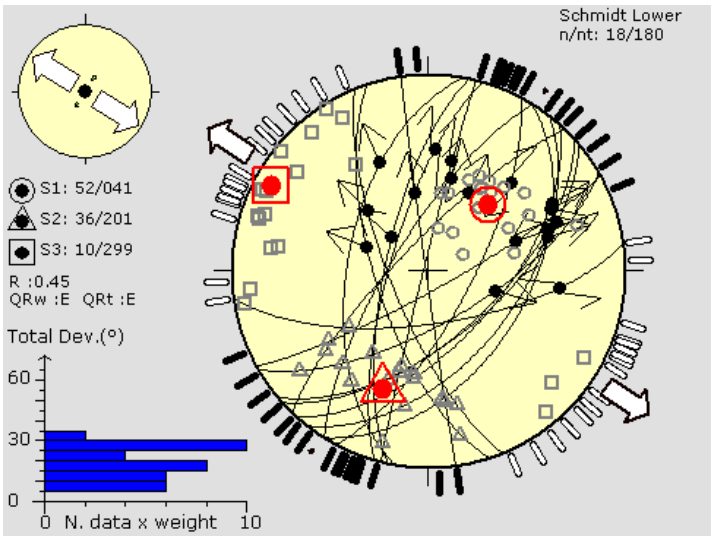


Fig. 18: NW-SE extension tensor

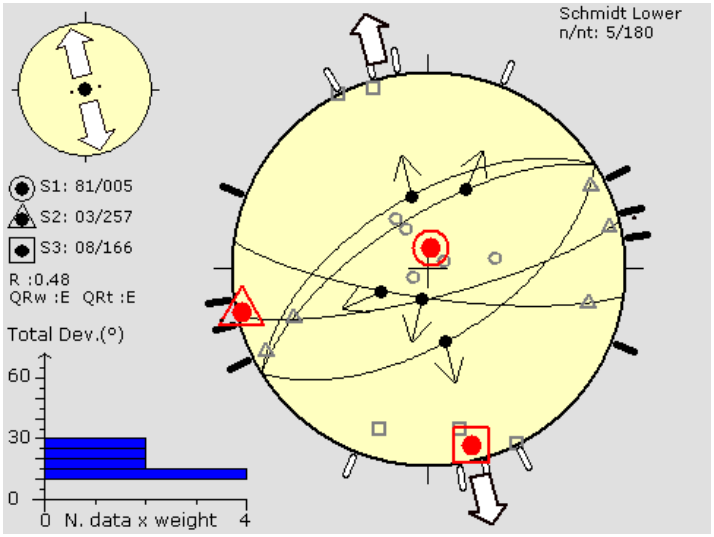


Fig. 19: NNW-SSE extension tensor.

**B-** Paleostress tensors according to Right dihedral (RHD) analysis:

Table 5: Elements of Paleostress Tensors in Study Area as a Whole Using Right Ddihedral (RHD) Analysis.

| No. | Faults no. | Principal stresses attitudes | | | R | R` | QRW | C.D | Tensor Type | δH max. | δH min. | Fig. |
|---|---|---|---|---|---|---|---|---|---|---|---|---|
| | | $\delta_1$ | $\delta_2$ | $\delta_3$ | | | | | | | | |
| 1 | 38 | 025/00 | 261/88 | 115/00 | 0.55 | 1.45 | D | 30 | P. Str | 025 | 115 | 20 |
| 2 | 37 | 062/06 | 291/79 | 153/07 | 0.51 | 1.49 | D | 24.6 | P. Str | 062 | 152 | 21 |
| 3 | 26 | 104/00 | 270/89 | 014/00 | 0.42 | 1.58 | E | 25.1 | P. Str | 104 | 014 | 22 |
| 4 | 11 | 308/15 | 184/63 | 044/20 | 0.36 | 1.64 | E | 22.7 | P.Str | 130 | 040 | 23 |
| 5 | 19 | 358/14 | 166/75 | 267/03 | 0.58 | 1.42 | E | 22.1 | P.Str | 178 | 088 | 24 |
| 6 | 7 | 028/01 | 298/12 | 126/77 | 0.43 | 2.43 | E | 20.5 | P.Com | 029 | 119 | 25 |
| 7 | 19 | 051/28 | 143/03 | 240/61 | 0.21 | 2.21 | E | 23.9 | St.com | 050 | 140 | 26 |
| 8 | 4 | 134/30 | 230/10 | 336/57 | 0.25 | 2.25 | E | 28.2 | P. com | 131 | 041 | 27 |
| 9 | 9 | 020/58 | 221/29 | 126/09 | 0.22 | 0.22 | E | 27.7 | R. Ext | 028 | 118 | 28 |
| 10 | 6 | 083/54 | 236/32 | 335/12 | 0.33 | 0.33 | E | 20.6 | P. Ext | 072 | 162 | 29 |

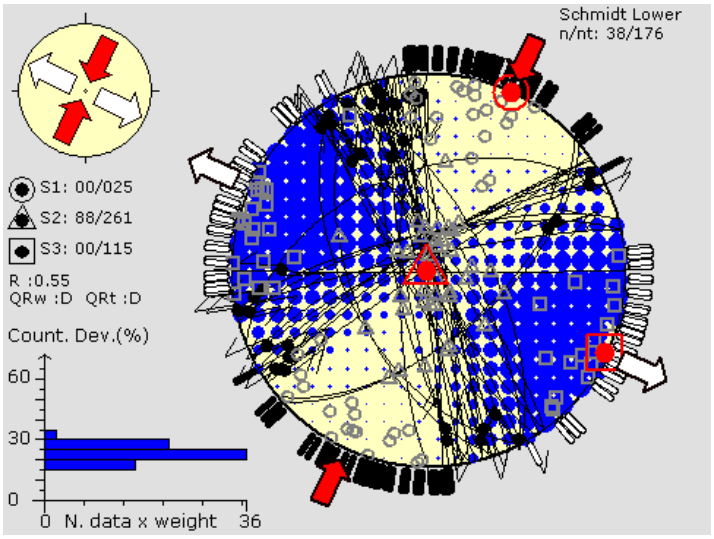


Fig. 20: NNE-SSW strike slip tensor

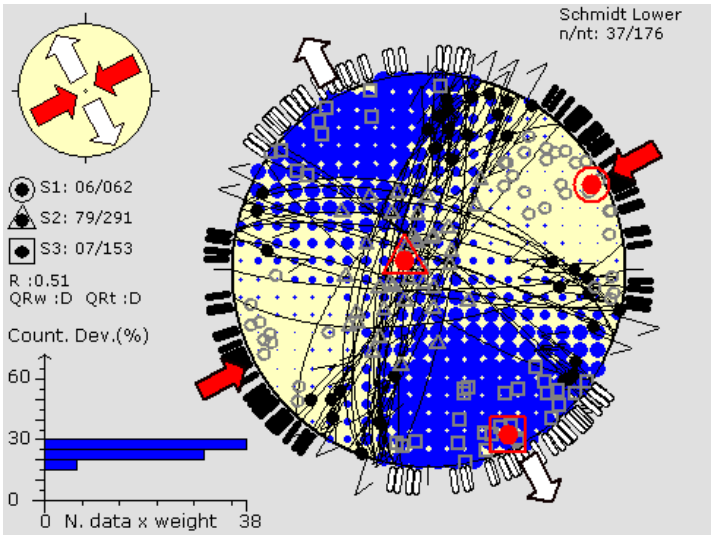


Fig. 21: NE-SW strike slip tensor

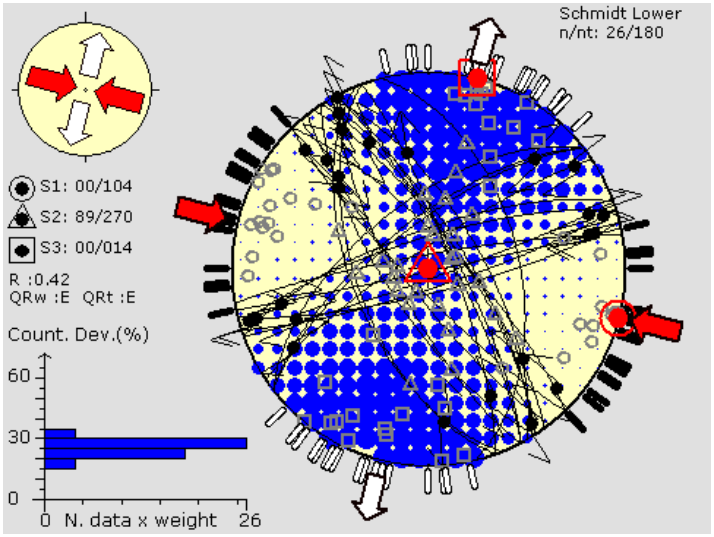


Fig. 22: WNW-ESE strike slip tensor

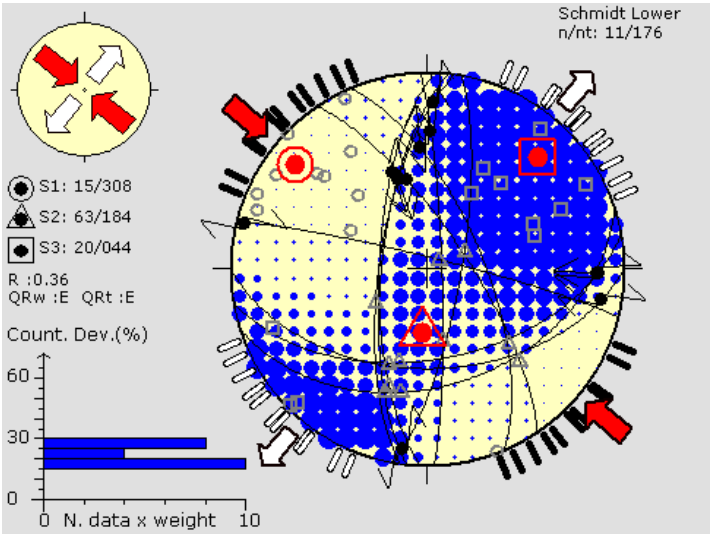


Fig. 23: NW-SE strike slip tensor

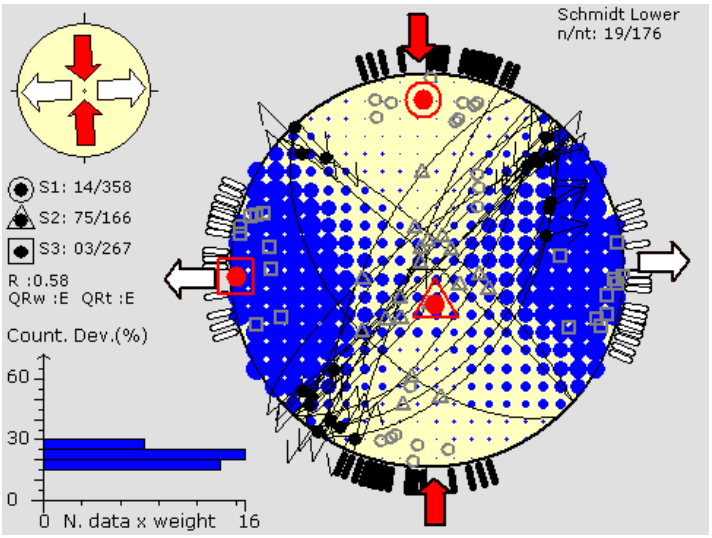


Fig. 24: NNW-SSE strike slip tensor

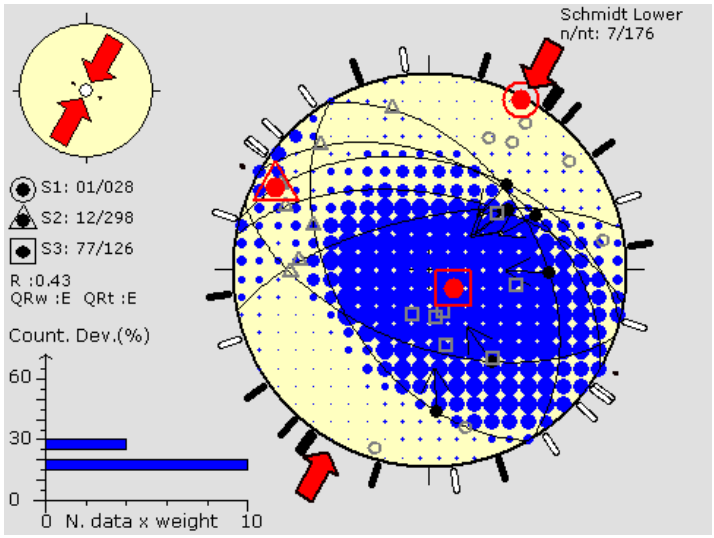


Fig. 25: NNE-SSW compressive tensor

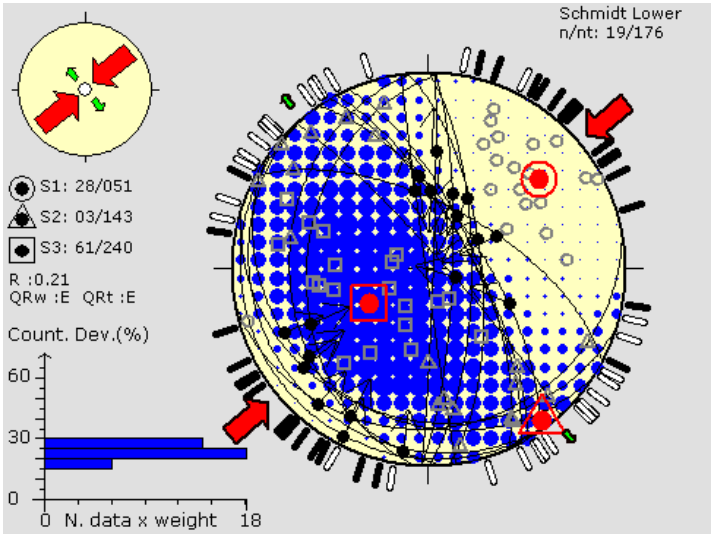


Fig. 26: NE-SW compressive tensor

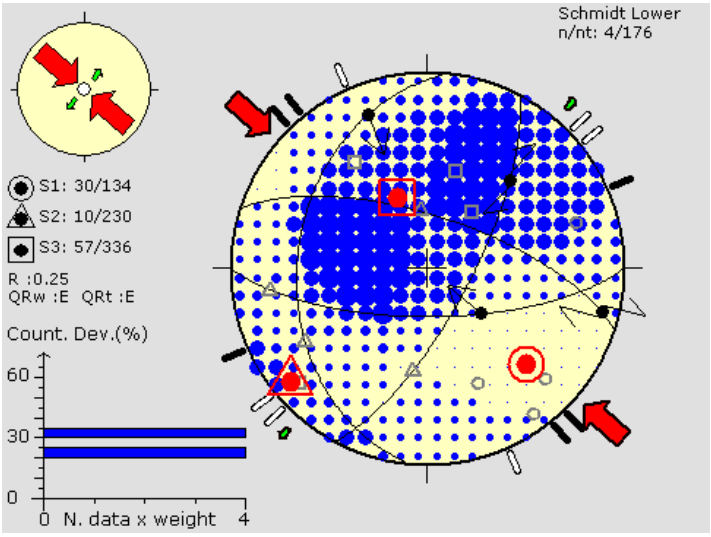


Fig. 27: NW-SE compressive tensor

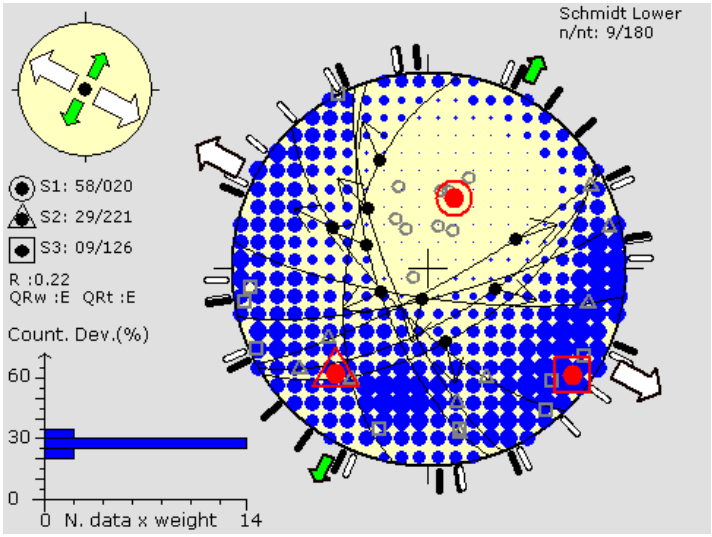


Fig. 28: NW-SE extension tensor

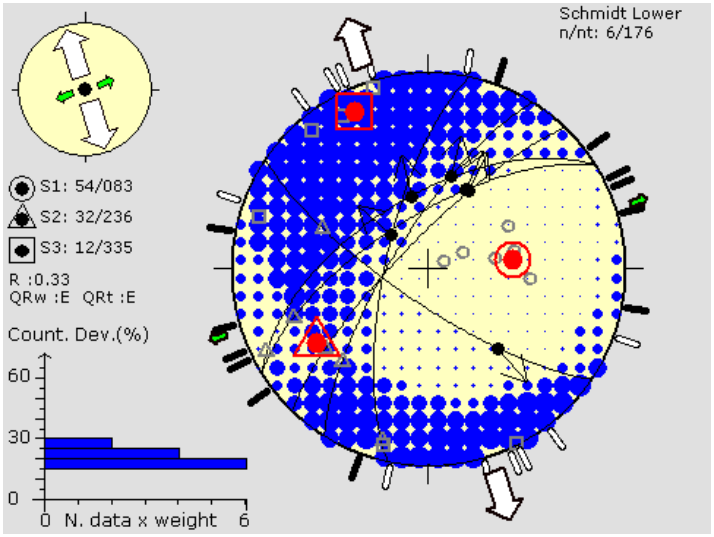


Fig. 29: NNW-SSE extension tensor

**Step 3**

In this final step, the output stress tensors of the step 2 were tested by the Rotational Optimization technique which is built in Win –Tensor software as well. Tables (6 and 7) and figures (30-47) demonstrate the final stress tensors got via optimization analysis. They are arranged according to the general azimuths of their greatest (strike slip and compressive tensors) and least (extension tensors) principal stress axes.

**A-** Optimized PBT Tensors:

Table 6: Paleostress Tensors after Rotational Optimization of the PBT output Tensors of Step 2 Aanalysis.

| No. | Faults no. | Principal stresses attitudes | | | R | R` | Q R W | α | WSM | δH max. | δH min. | Fig. |
|---|---|---|---|---|---|---|---|---|---|---|---|---|
| | | $\delta_1$ | $\delta_2$ | $\delta_3$ | | | | | | | | |
| 1 | 11 | 009/12 | 137/70 | 276/14 | 0.41 | 1.59 | E | 8.91 | SS | 008 | 098 | 30 |
| 2 | 54 | 026/01 | 123/80 | 296/09 | 0.1 | 1.9 | C | 13.9 | SS | 026 | 116 | 31 |
| 3 | 12 | 236/04 | 345/76 | 145/12 | 0.26 | 1.74 | E | 16.6 | SS | 056 | 146 | 32 |
| 4 | 31 | 279/01 | 020/85 | 189/04 | 0.03 | 1.97 | D | 11.1 | SS | 100 | 010 | 33 |
| 5 | 19 | 309/22 | 171/60 | 047/17 | 0.3 | 1.7 | E | 13.2 | SS | 132 | 042 | 34 |
| 6 | 20 | 052/16 | 319/08 | 203/71 | 0.42 | 2.42 | E | 11.6 | TF | 054 | 144 | 35 |
| 7 | 8 | 349/07 | 256/25 | 093/63 | 0.2 | 2.2 | E | 14.1 | TF | 171 | 081 | 36 |
| 8 | 7 | 087/72 | 302/14 | 210/09 | 0.19 | 0.19 | E | 17.3 | NF | 111 | 021 | 37 |
| 9 | 18 | 054/49 | 202/35 | 305/16 | 0.04 | 0.04 | E | 10.7 | NS | 054 | 144 | 38 |

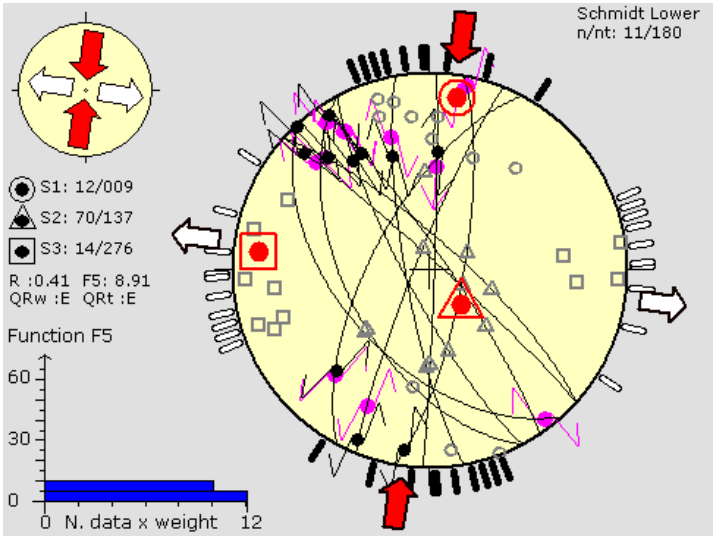


Fig. 30: NNE-SSW strike slip tensor

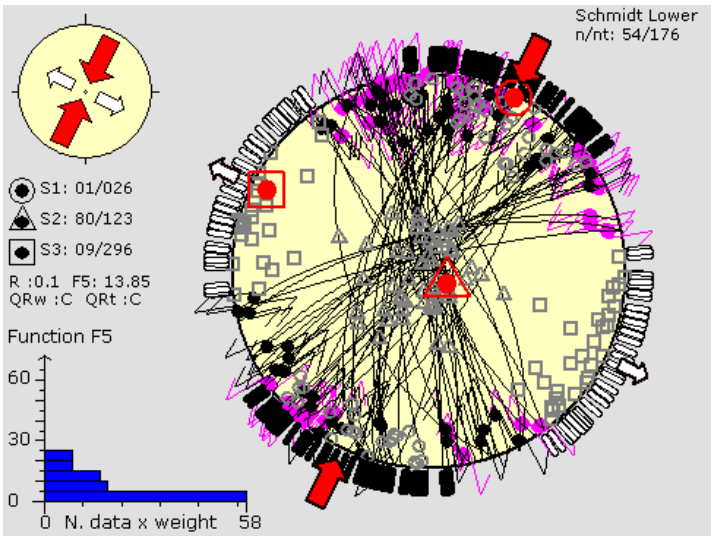


Fig. 31: NNE-SSW strike slip tensor

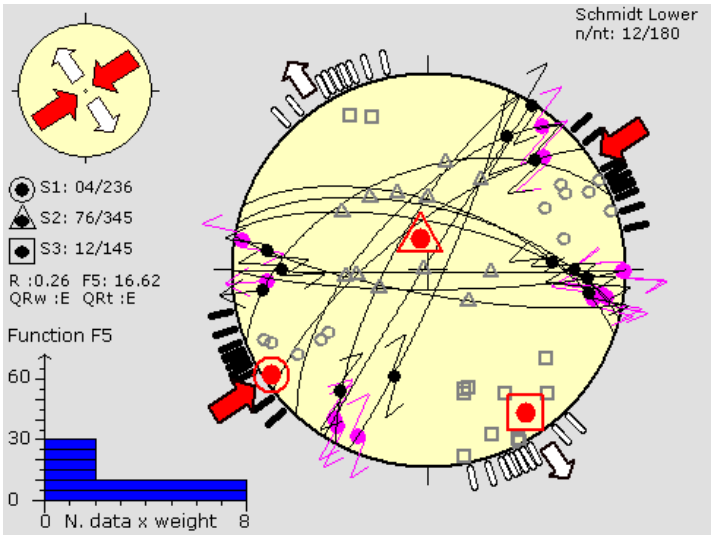


Fig. 32: NE-SW strike slip tensor

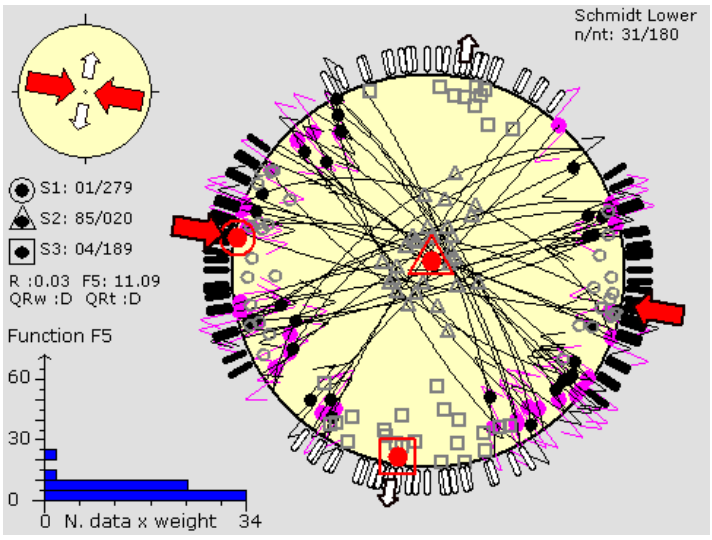


Fig. 33: WNW-ESE strike slip tensor

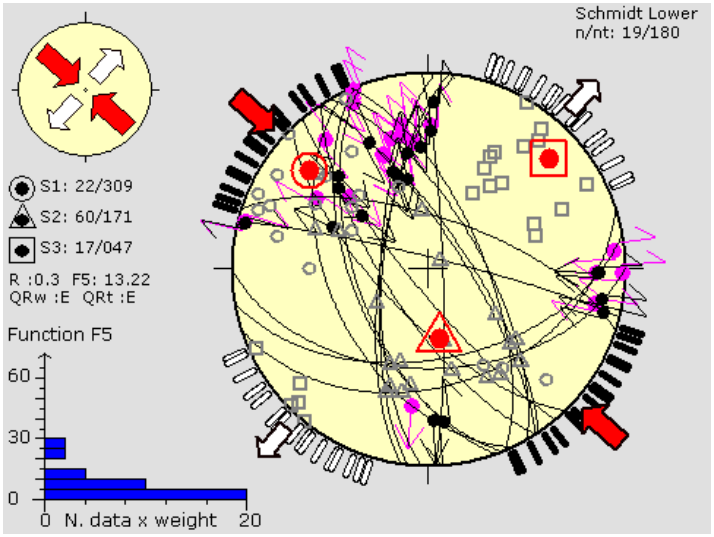


Fig. 34: NW-SE strike slip tensor

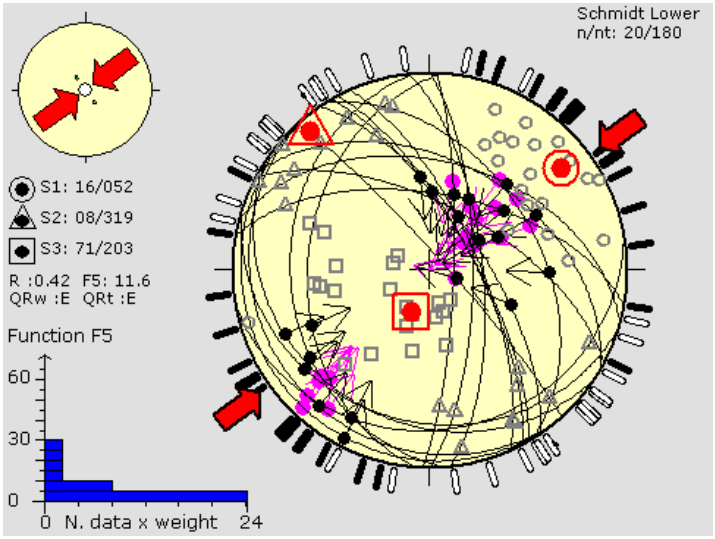


Fig. 35: NE-SW compressive tensor

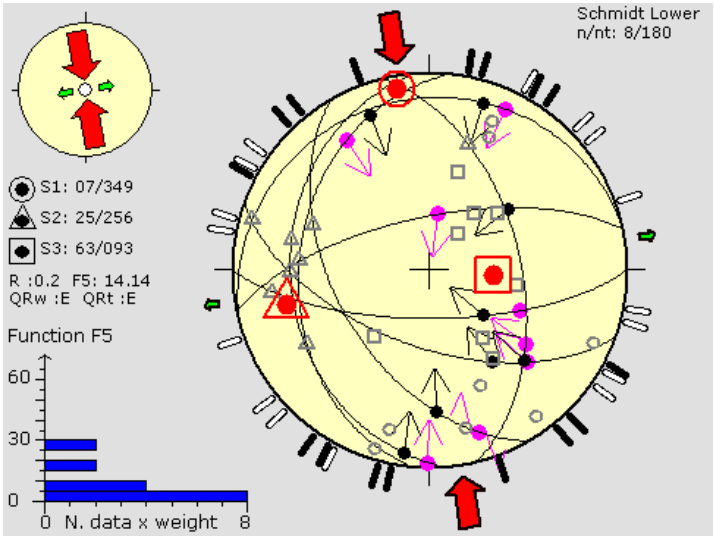


Fig. 36: NNW-SSE compressive tensor

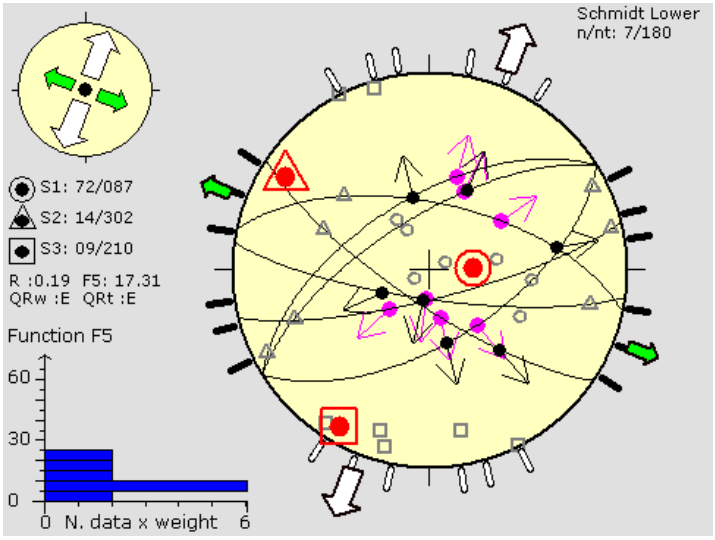


Fig. 37: NNE-SSW extension tensor

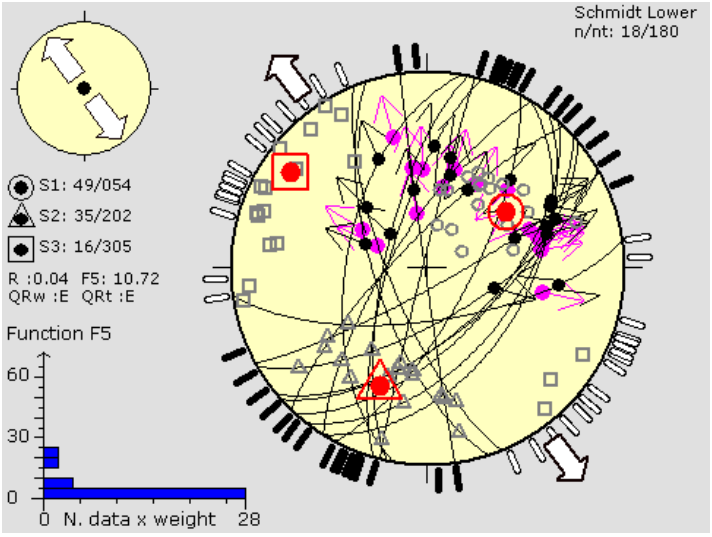


Fig. 38: NW-SE extension tensor

**B-** Optimized RHD Tensors:

Table 7: Paleostress Tensors after Rotational Optimization of the RDH output Tensors of Step 2 Analysis.

| No. | Faults no. | Principal stresses attitudes | | | R | R` | Q R W | α | WSM | δH max. | δH min. | Fig. |
|---|---|---|---|---|---|---|---|---|---|---|---|---|
| | | $\delta_1$ | $\delta_2$ | $\delta_3$ | | | | | | | | |
| 1 | 19 | 007/20 | 178/68 | 276/03 | 0.57 | 1.43 | E | 11.68 | SS | 007 | 097 | 39 |
| 2 | 37 | 026/07 | 171/81 | 296/05 | 0.68 | 1.32 | D | 10.45 | SS | 027 | 117 | 40 |
| 3 | 35 | 063/12 | 258/77 | 154/03 | 0.42 | 1.58 | D | 14.12 | SS | 064 | 154 | 41 |
| 4 | 23 | 285/03 | 188/62 | 016/27 | 0.17 | 1.83 | E | 10.77 | SS | 105 | 015 | 42 |
| 5 | 13 | 317/19 | 183/62 | 053/18 | 0.36 | 1.64 | E | 10.53 | SS | 140 | 050 | 43 |
| 6 | 24 | 043/26 | 306/13 | 192/60 | 0.3 | 2.3 | E | 11.8 | TF | 046 | 136 | 44 |
| 7 | 5 | 125/02 | 215/12 | 033/46 | 0.79 | 2.79 | E | 8.44 | TS | 125 | 035 | 45 |
| 8 | 4 | 317/53 | 166/33 | 066/13 | 0.06 | 0.06 | E | 6.03 | NF | 140 | 050 | 46 |
| 9 | 11 | 025/75 | 250/10 | 158/09 | 0.1 | 0.1 | E | 15.8 | NF | 055 | 145 | 47 |

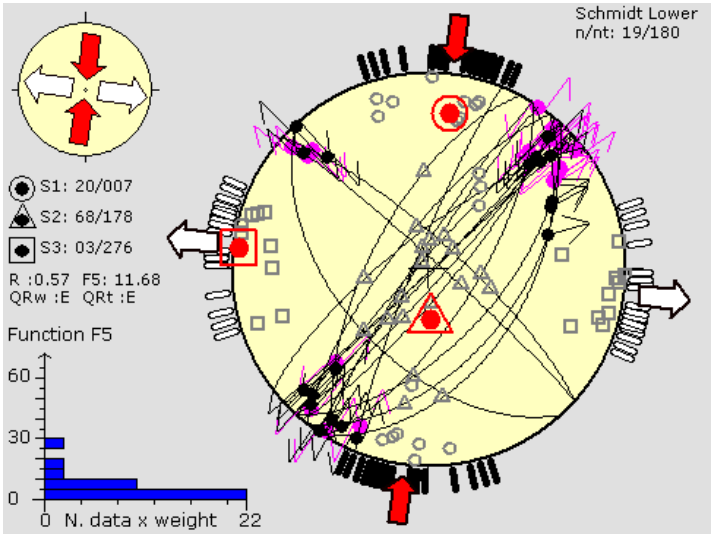


Fig. 39: NNE-SSW strike slip tensor

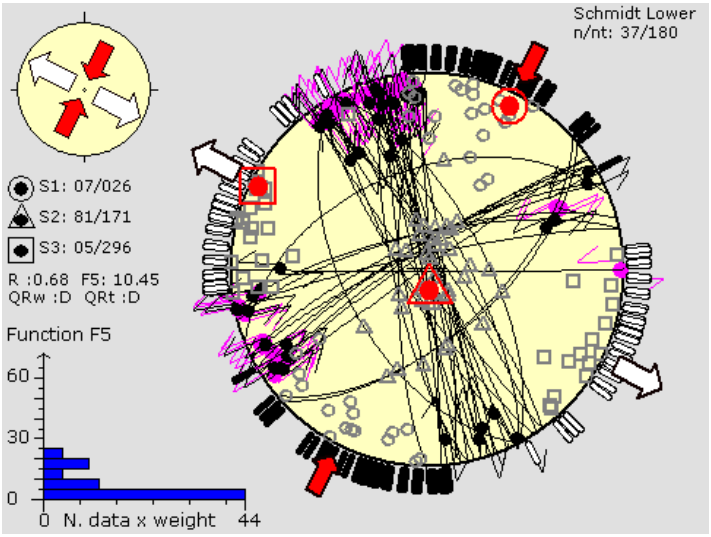


Fig. 40: NNE-SSW strike slip tensor

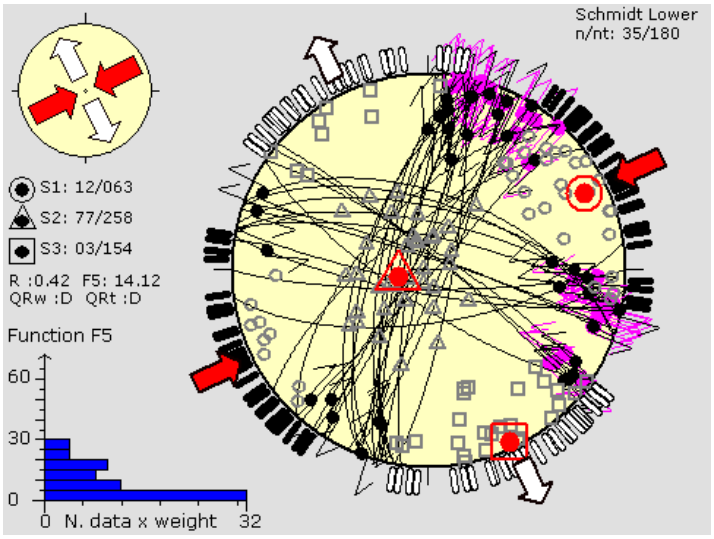


Fig. 41: NE-SW strike slip tensor

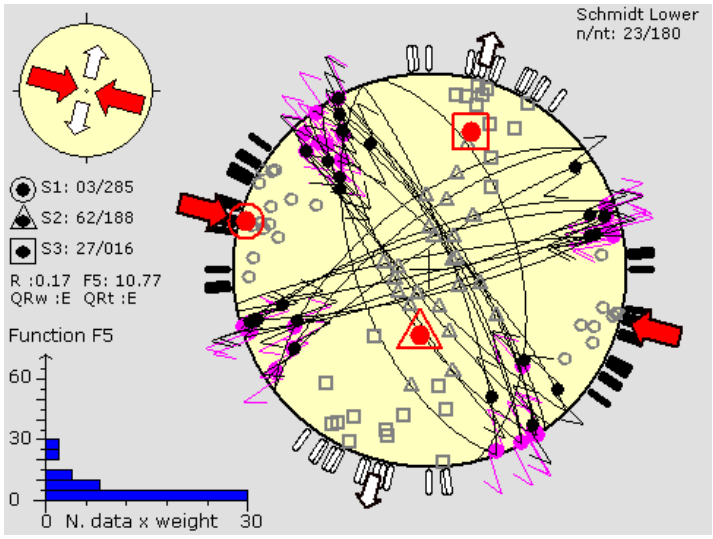


Fig. 42: WNW-ESE strike slip tensor

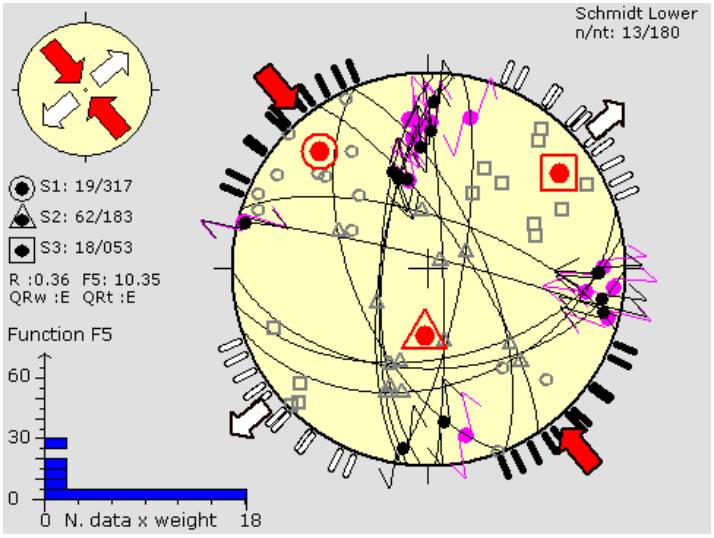


Fig. 43: NW-SE strike slip tensor

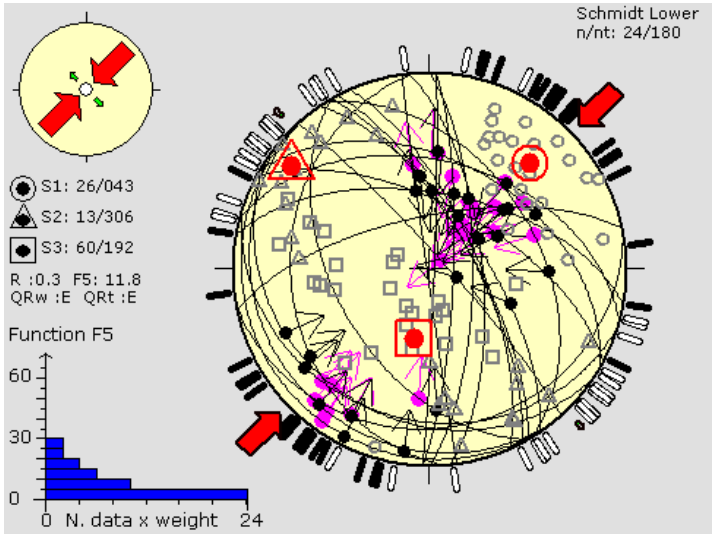


Fig. 44: NE-SW compressive tensor

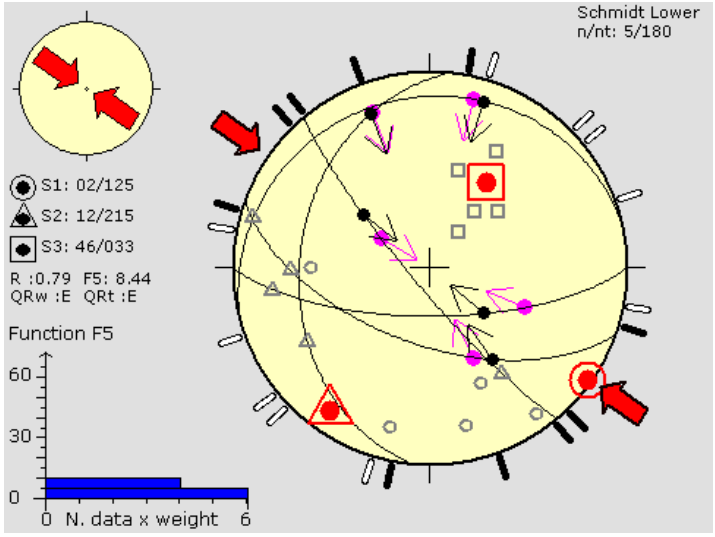


Fig. 45: NW-SE compressive tensor

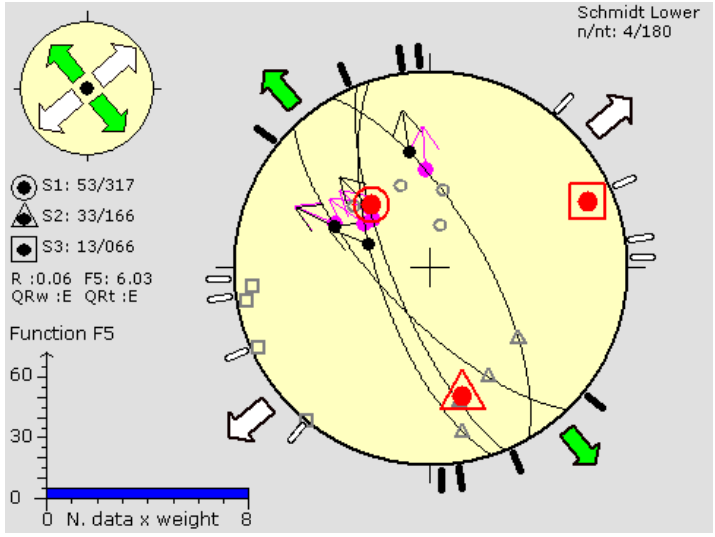


Fig. 46: NE-SW extension tensor

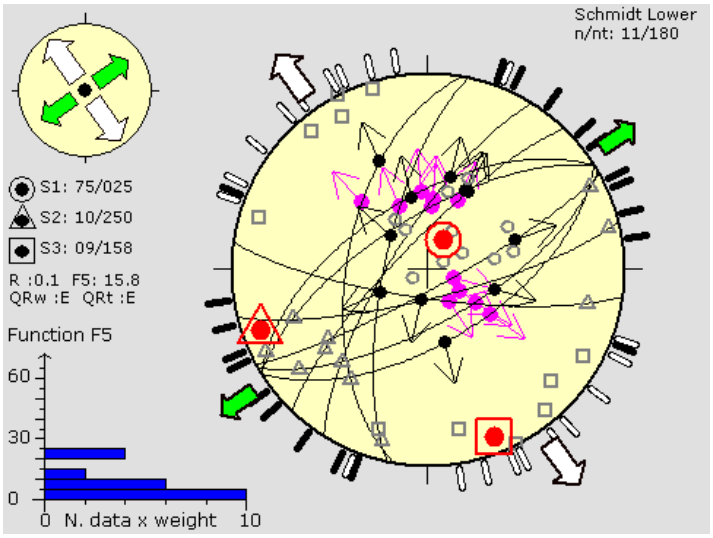


Fig. 47: NW-SE extension tensor

## TECTONIC INTERPRETATION

The successive kinematic analysis of (180) fault slip data, distributed throughout (10) field stations at Sara anticline northeastern Iraq, had revealed numerous paleostress tensors of varied types, orientation and strength. They are listed hereafter according to the general azimuths of their greatest principal stress axes ($\sigma_1$) for strike slip (Table 8) and compressive tensors (Table 9), and least principal stress axes ($\sigma_3$) for extensional tensors (Table 10).

Table 8: Relative Prevalence of Strike Slip Paleostress Tensors Throughout Three Steps of Fault Slip Analysis in Study Area. Figures in the Fields Represent Fault Numbers, Those in Parenthesis are Bearings of Horizontal Maximum Principal Stress Axis (**δH max.**) of Tensors.

| **$\sigma_1$ Azimuth** | **Number of faults** | | | | |
|---|---|---|---|---|---|
| | **Step 1 P.B.T** | **Step 2 P.B.T** | **Step 2 R.H.D** | **Step 3 ROP1** | **Step 3 ROP2** |
| NNE-SSW | 52 | 58(024) | 38(025) | 11(008),54(026) | 19(007),37(027) |
| NE-SW | 24 | 10(062) | 37(062) | 12(056) | 35(064) |
| ENE-WSW | 18 | | | | |
| WNW-ESE | 18 | 34(099) | 26(104) | 31(100) | 23(105) |
| NW-SE | 9 | 15(132) | 11(130) | 19(132) | 13(140) |
| NNW-SSE | 10 | 7(169) | 19(178) | | |

Table 9: Relative Prevalence of Compressive Paleostress Tensors Throughout three Steps of Fault Slip Aanalysis in Study Area. Figures in the Fields Represent Fault Numbers, those in Parenthesis are Bearings of Horizontal Maximum Principal Stress Axis (**δH max.)** of Tensors.

| **$\sigma_1$ Azimuth** | **Number of faults** | | | | |
|---|---|---|---|---|---|
| | **Step 1 P.B.T** | **Step 2 P.B.T** | **Step 2 R.H.D** | **Step 3 ROP1** | **Step 3 ROP2** |
| NNE-SSW | 2 | 9(034) | 7(029) | | |
| NE-SW | 17 | 15(051) | 19(050) | 20(054) | 24(046) |
| ENE-WSW | 2 | | | | |
| WNW-ESE | 2 | 1(118) | | | |
| NW-SE | 5 | 3(147) | 4(131) | | 5(125) |
| NNW-SSE | 2 | | | 8(171) | |

Table 10: Relative Prevalence of Extension Paleostress Tensors Throughout three Steps of Fault Slip Analysis in Study Area. Figures in the Fields Represent fault numbers, those in parenthesis are bearings of horizontal minimum principal stress axis (**δH min.)** of tensors.

| **$\sigma_3$ Azimuth** | **Number of faults** | | | | |
|---|---|---|---|---|---|
| | **Step 1 P.B.T** | **Step 2 P.B.T** | **Step 2 R.H.D** | **Step 3 ROP1** | **Step 3 ROP2** |
| NNE-SSW | 4 | 3(030) | | 7(021) | |
| NE-SW | 5 | | | | 4(050) |
| ENE-WSW | 1 | 2(070) | | | |
| WNW-ESE | 2 | 18(123) | 9(118) | | |
| NW-SE | 7 | | | 18(144) | 11(145) |
| NNW-SSE | | 5(166) | 6(162) | | |

It is clear from the tables listed above that the strike slip tensors are most prevalent than either of compressive and extension tensors. However the number of tensors has been reduced successively from step (1) analysis towards steps (2) and (3). This is because the data available at either field station for step (1) analysis is much less than the whole data used in the successive steps of analysis. Therefore the results of step (3) analysis seem more reliable. The NNE-SSW, NE-SW, WNW-ESE and NW-SE are more conspicuous and prevalent than others among the strike slip tensors, whereas the NE-SW is predominant among compressive tensors. However among extension tensors, the NW-SE one is more prevalent than the rest.

Moreover, some of above cited stress tensors were verified also by analysis of other available kinematic indicators in the study area. These are pressure solution surfaces (stylolite seams), tension fractures, veins and conjugate shear fractures. Four sets of stylolite seams indicate a predominant (NNE-SSW) and subordinate (NNW-SSE, E-W, NW-SE) compression directions (Fig. 48). A predominant (NW-SE) and subordinate (NNE-SSW, NE-SW, ENE-WSW, E-W) extension directions were deduced from planar tension fractures and veins (Fig. 49). NNW-SSE compressive direction detected from conjugate shear fractures (Fig. 50). NE-SW directed compressive stress axis extracted from conjugate hko shear fractures acute about **a** tectonic axis (Fig. 51). Furthermore, the impact of WNW- ESE- strike slip stress tensor is quite clear in development of transversal minor folds in Gercus and Pila Spi formations at SW limb of the main anticline (station 5, Photo 7).


Photo 7: A transverse minor fold within Gercus Fm. at SW limb of Sara Anticline developed due to stress tensor sub parallel with the main anticline trend.

The prevalence of strike slip tensors among other paleostress tensors in study area might be attributed to the oblique convergence and collision of Arabian and Eurasian (Iranian) plates (Numan, 1997; 2001a; 2001b; Alavi, 2004; 2007; Agard *et al.,* 2005; Authemayou *et al.,* 2006). The progressive oblique collision (dextral transpression) led to partitioning of the instantaneous stress vector into normal and tangential components with respect to the boundary between the colliding plates. And because the margins of collided continents were actually arched and zigzagged, so the orientations of resultant stress vector components varied in space and time during such progressive collision between the respective plates.

However, strike slip and compressive tensors other than NNE-SSW and NE-SW (normal or subnormal to the main fold trend), might represent secondary tensors related to relaxation episode that succeeded the primary tectonic compressive pulse. The attitudes of greatest and least principal stress axes were permutated in such relaxed tensors relative to their attitudes in primary tensors (Angelier, 1989). The NW-SE extension tensor is secondary byproduct of the primary compressive pulse. Whereas, the NNE-SSW and NE-SW extension tensors might refer to the releasing phase which accompanied the final uplift of the main fold.

The association of pitted (stylolite peaks) and striated (shear) sectors in some strike slip fault planes (station 1, Photo 4) demonstrates the transpressive character of the primary NNE-SSW stress tensor. That is $\sigma_{Hmax.}$ of both striated and pitted sectors are almost identical in orientation. Meanwhile, the juxtaposition of the calcite crystal growth facet with striated (shear) facet on the some strike slip fault planes (station 1, Photo 5) illustrates the transtensive character of the other primary NE-SW stress tensor. That is $\sigma_{Hmin.}$ of both striated and calcite coated facets are coincident in orientation. Both transpressive and transtensive characteristics of mesofaults and hence their causative stress tensors might be considered as signs for oblique collision of Arabian and Eurasian tectonic plates in this region.

The superimposition of striation sets on mesofault planes in some localities might give some clues about relative chronological relationship between certain stress tensors deduced in the present investigation. For instance in station (6), the same fault plane bears a relatively younger striation set indicating normal slip superimposed on an older set indicating reverse slip. Thus the NE-SW extension stress tensor deduced by the relatively younger striation set might considered as a successive releasing state for the primary NE-SW compressive stress tensor deduced from the relatively older striation set on the same fault. A similar chronological relationship is evident on another mesofault plane in the same locality; an older striation set indicates a primary NNE-SSW strike slip stress tensor whereas the relatively younger set refers to a secondary relaxed WNW-ESE strike slip tensor after permutation of principal stress axes with the former primary stress tensor. At station (4); a strike slip fault bearing two superimposed striation sets indicate that the WNW-ESE strike slip stress tensor which is (a secondary relaxation tensor after the primary NNE-SSW strike slip tensor), is relatively older than the primary NE-SW strike slip tensor. At station (4) also, a reverse slip mesofault bears two superimposed striation sets indicating a relatively younger NE-SW primary compressive tensor than the earlier NNE-SSW primary compressive stress tensor. This might be attributed to the counterclockwise rotation of Arabia during its oblique collision against Eurasia.


Fig. 48: Compression axes as indicated by peaks of stylolite seams in study area. **a**- NNW-SSE and NNE-SSW, **b**- E-W, NW-SE compression directions.

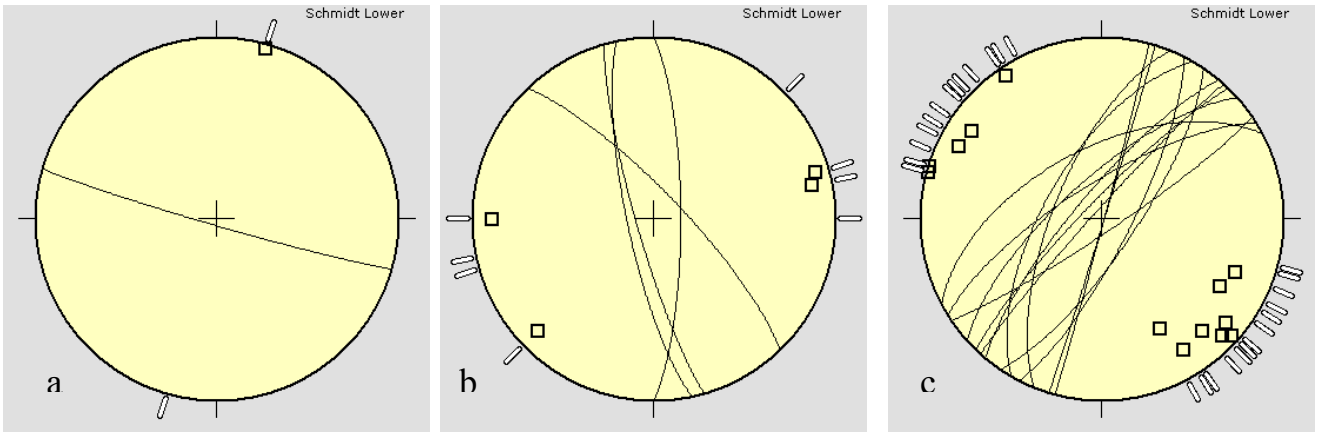


Fig. 49: Extension axes as indicated by poles of extension fractures and veins in study area. **a-** NNE-SSW, **b-** NE-SW, ENE-WSW, E-W and **c-** NW-SE extension directions.

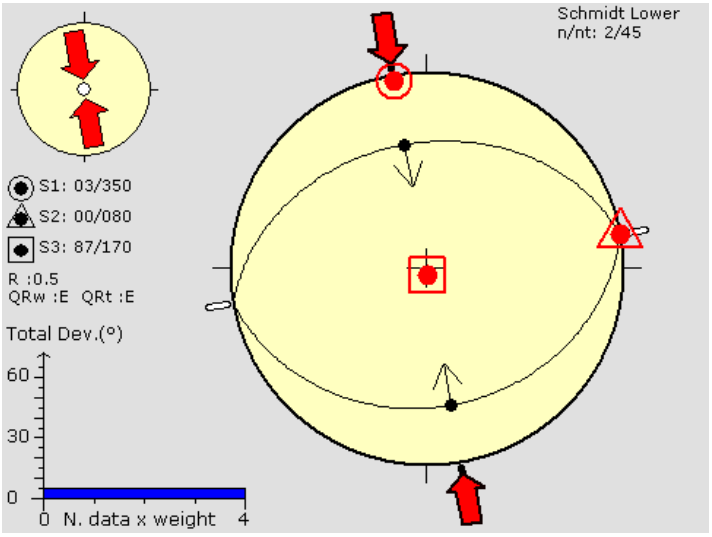


Fig. 50: NNW-SSE compression derived by conjugate shear fractures.

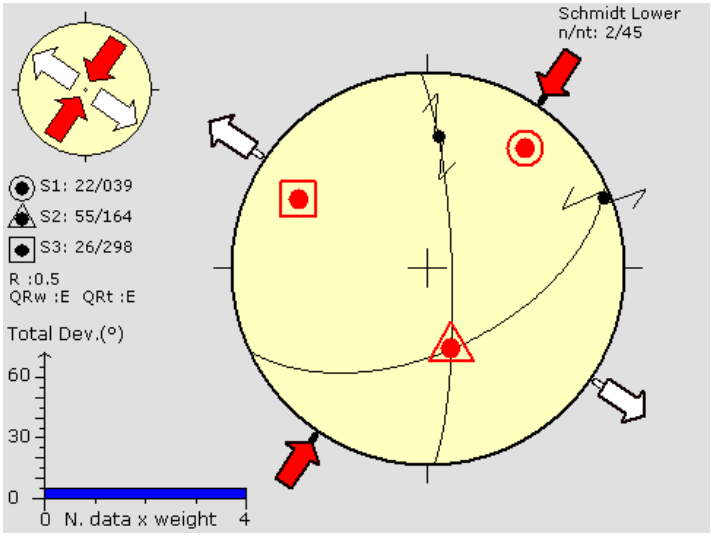


Fig. 51:NE-SW strike slip by conjugate hko >a shear fractures.

## CONCLUSIONS

The present faults slip analysis at Sara Anticline revealed the following conclusions:

1- Primary strike slip and compressive stress states with their maximum horizontal axes ($\sigma_{Hmax.}$) in NNE-SSW, NE-SW directions.
2- These stress directions might be attributed to the progressive oblique collision of Arabian and Eurasian (Iranian) plates.
3- The WNW-ESE, NW-SE strike slip and compressive tensors (according to their $\sigma_{Hmax}$ general trends), considered as secondary stress tensors developed in relaxation episode succeeding the primary compressive pulse.
4- The NW-SE extension stress tensor (according to the $\sigma_{Hmin.}$ general trend), regarded as an extension byproduct of the primary NE-SW compressive stress tensor. However the NNE-SSW and NE-SW extension tensors might be related to the releasing phase that accompanied the final uplift of the main fold.
5- The stress tensors extracted by analysis of fault slip data in study area were verified by kinematic indicators such as stylolite seams, planar veins and extension fractures and conjugate shear fractures**.**

## REFERENCES

Agard, P., Omrani, J., Jolivet, J., and Mouthereau, F., 2005. Convergence History Across Zagros (Iran): Constraints from Collisional and Earlier Deformation: International Journal of Earth Sciences, Vol. 94, pp. 401 - 419.

Alavi, M. 2004. Regional Stratigraphy of the Zagros Fold-Thrust Belt of Iran and its Proforeland Evolution. Am. Jour. Sci., Vol. 304, pp. 1 - 20.

Alavi, M. 2007. Structures of the Zagros Fold-Thrust Belt in Iran. Am. Jour. Sci., Vol. 307, pp. 1067 - 1095.

Angelier, J. and Mecheler, P., 1977. Surune Methode Graphique, de Recbercbe Des Contraintes en Seismologie: La Methode de Diedres Droits. Pull. Soc. Geol. France, Vol, 7, pp. 1309 - 1318.

Angelier, J., Tarantola, A., Manoussis, S., Valette, B., 1982. Inversion of Field Data in Fault Tectonics to Obtain the Regional Stress. Geophysical Journal of the Royal Astronomical Society, Vol. 69, pp. 607 - 621.

Angelier, J., 1984. Tectonic Analysis of Fault-Slip Ddata Sets. Journal of Geophysical Research, Vol. 89, pp. 5835 - 5848.

Angelier, J., 1989. From Orientation to Magnitudes in Paleostress Ddetermination using Fault Slip Data. Journal of Structural Geology, Vol. 11, pp. 37 - 50.

Angelier, J., 1990. Inversion of Field Data in Fault Tectonics to Obtain Regional Stress. III. A new Rapid Direct Inversion Method by Analytical Means. Geophysical Journal International, Vol. 103, pp. 363 - 376.

Angelier, J., 1994. Fault Slip Analysis and Paleostress Rreconstruction. In: Hancock, P.L. (Ed.), Continental Deformation. Pergamon Press, Oxford, pp. 53 - 100.

Authemayou, C., Chardon, D., Bellier, O., Malekzadeh, Z., Shabanian, E., and Abbassi, M. R., 2006. Late Cenozoic Partitioning of Oblique Plate Convergence in the Zagros Fold and Thrust Belt (Iran).Tectonics, 25, TC, 3002.

Bott, M. P. H., 1959. The Mechanics of Oblique-Slip Faulting. Geological Magazine, Vol. 96, pp. 109 - 117.

Delvaux, D. and Sperner, B., 2003. Stress Tensor Inversion from Fault Kinematic Indicators and Focal Mechanism Data. The TENSOR Program. In: New Insights into Structural Interpretation and Modeling (D. Nieuwland Ed.); Geol. Soc. London, Special Publications, Vol. 212, pp. 75 - 100.

Jassim, S. Z. and GOFF, J. C. 2006. Geology of Iraq. Dolin, Prague and Moravian Museum, Brno, 341 p.

Krantz, R.W., 1988. Multiple Fault Sets and Three - Dimensional Strain: theory and Application. Journal of Structural Geology, Vol. 10, pp. 225 - 237.

Nemcok, M., Lisle, R. J., 1997. A Stress Inversion Procedure for Polyphase Fault/Slip Data Sets. Journal of Structural Geology, Vol. 17, pp. 1445 - 1453.

Numan, N. M. S. 1997. A plate Tectonic Scenario for the PhaneroZoic Succession in Iraq. Iraqi Geol. Jour., Vol. 30, 85 p.

Numan, N. M. S., 2001a. Cretaceous and Tertiary Alpine Subductional History in Northern Iraq. Iraqi Jour. Earth Sci., Vol. 1, No. 2, pp. 59 - 74.

Numan, N. M. S., 2001b. Discussion on "Dextral Transpression in Late Cretaceous Continental Collision, Sanandaj - Sinjar Zone, Western Iran". J. Struct. Geol., Vol. 23.

Pollard, D. D., Saltzer, S. D., Rubin, A. M., 1993. Stress Inversion Methods: are they Bbased on Faulty Aassumptions. Journal of Structural Geology, Vol. 15, pp. 145 - 154.

Twiss, R. J., Unruh, J. R., 1998. Analysis of Fault Slip Inversion: do they Constrain Stress or Strain rate. Journal of Geophysical Research, Vol. 103 (B6), pp. 12205 - 12222

Wallace, R. E., 1951. Geometry of Shearing Stress and Relation to Faulting. Journal of Geology, Vol. 69, pp. 118 - 130.